Helmholtz-Zentrum Geesthacht

Materials Mechanics

A thermodynamically and variationally consistent
class of damage-type cohesive models

J. Mosler and I. Scheider

A thermodynamically and variationally consistent class of damage-type cohesive models

J. Mosler & I. Scheider

Materials Mechanics
Institute of Materials Research
Helmholtz-Zentrum Geesthacht
D-21502 Geesthacht, Germany
E-Mail: joern.mosler@hzg.de

SUMMARY

A novel class of cohesive constitutive models suitable for the analysis of material separation such as that related to cracks, shear bands or delamination processes is presented. The proposed framework is based on a geometrically exact description (finite deformation) and it naturally accounts for material anisotropies. For that purpose, a Helmholtz energy depending on evolving structural tensors is introduced. In sharp contrast to previously published anisotropic cohesive models with finite strain kinematics based on a spatial description, all models belonging to the advocated class are thermodynamically consistent, i.e., they are rigorously derived by applying the Coleman & Noll procedure. Although this procedure seems nowadays to be standard for stress-strain-type constitutive laws, this is not the case for cohesive models at finite strains. An interesting new finding from the Coleman & Noll procedure is the striking analogy between cohesive models and boundary potential energies. This analogy gives rise to the introduction of additional stress tensors which can be interpreted as deformational surface shear. To the best knowledge of the authors, those stresses which are required for thermodynamical consistency at finite strains, have not been taken into account in existing models yet. Furthermore, the additional stress tensors can result in an effective traction-separation law showing a non-trivial stress-free configuration consistent with the underlying Helmholtz energy. This configuration is not predicted by previous models. Finally, the analogy between cohesive models and boundary potential energies leads to a unique definition of the controversially discussed fictitious intermediate configuration. More precisely, traction continuity requires that the interface geometry with respect to the deformed configuration has to be taken as the average of both sides. It will be shown that the novel class of interface models does not only fulfill the second law of thermodynamics, but it also shows an even stronger variational structure, i.e., the admissible states implied by the novel model can be interpreted as stable energy minimizers. This variational structure is used for deriving a variationally consistent numerical implementation.

1 Introduction

Since the early work by Barenblatt [1] on quasi-brittle materials (see also [2]) and that by Dugdale [3] on ductile metals, *cohesive interface models* represent one of the most powerful and versatile tools available for the analysis of material failure. Within such models, cohesive tractions (stress vector acting at a crack), usually given in terms of the crack width (displacement discontinuity), resist the separation of the bulk material across the crack. Accordingly, they are based on stress-displacement laws (instead of a classical stress-strain-relationship). This is why they are often referred to as *traction-separation laws*. One of the most important advantages of such discrete representations of material failure is that the width of the respective failure zone is approximated as zero (with respect to the undeformed configuration) and thus, the length scale associated with material failure is a priori infinitely smaller than that of the considered structure. As a result, cohesive interface models are intrinsically multiscale approaches, cf. [4]. Another important advantage of interface models when combined with continuum approaches is their naturally induced size effect, cf. [5] (see also [6]). For a more detailed analysis of the physical properties related to interface models, the interested reader is referred to [4].

While the number of different cohesive interface models in the literature is tremendous (for an overview, see [7, 8] and references cited therein), interface laws specifically designed for material failure at finite strains are still relatively rare – particularly for anisotropic solids. However, geometrically nonlinear effects and anisotropic mechanical responses do play an important role in many applications, e.g., in delamination processes, cf. [9].

Roughly, geometrically exact cohesive models can be subdivided into two groups. The first group of such interface models originally developed for slip bands (mode-II or mode-III failure) is based on the so-called *material displacement discontinuity*, cf. [10, 11] (see also [12–18]). Conceptually, instead of using the displacement jump $[\![u]\!]$ itself, its pull-back $J = F^{-1} \cdot [\![u]\!]$ is employed. Usually, although not mandatory, it is assumed that the

1

localized deformations $\boldsymbol{J}$ are of purely irreversible, plastic nature. In line with classical plasticity theory (stress-strain relation), they only occur, if a stress-based criterion is fulfilled (depending on a yield function) and they are governed by evolution equations similar to those of the plastic strains. Clearly, by using a referential description, the requirements imposed by the principle of objectivity are a priori fulfilled. Furthermore, the analogy to classical continuum plasticity theories makes it possible to apply already existing powerful and well established techniques such as the Coleman & Noll procedure, cf. [19, 20]. For this reason, models falling into the range of this class are relatively well developed and thermodynamically consistent, e.g., they comply with the constraints imposed by the second law of thermodynamics.

Although the aforementioned group of interface models seems to be very promising, it is not well suited for some applications. The first reason is rather technical: From a materials science point of view, it is more natural to work with true stresses and true displacements (instead of using a referential description). The second point is, however, more crucial: Using the material displacement discontinuity within constitutive laws implies that the physical displacement jump consists of an additional convective term, i.e., $[\![\dot{\boldsymbol{u}}]\!] = \dot{\boldsymbol{F}} \cdot \boldsymbol{J} + \boldsymbol{F} \cdot \dot{\boldsymbol{J}}$ (Here, the superposed dot denotes the material time derivative.). Accordingly, even for an unloading process ($\dot{\boldsymbol{J}} = \boldsymbol{0}$), the length of the physical displacement jump may change, i.e., ($\dot{\boldsymbol{J}} = \boldsymbol{0} \;\;\not\Rightarrow\;\; ||\,[\![\dot{\boldsymbol{u}}]\!]\,|| = 0$). This effect is similar to that known from classical finite strain plasticity theory based on an evolution equation formulated within the intermediate configuration. Depending on the underlying failure process, it can be desired (for ductile plastic slip) or unphysical (for quasi-brittle materials).

For quasi-brittle materials, the second group of interface models is more suitable. In contrast to the aforementioned framework, it is based on a traction-separation law described with respect to the current, i.e., deformed, configuration. Consequently, the introduction of the material displacement discontinuity is not required. Models representative of this class can be found, e.g., in [9, 21–24]. Clearly, the constraints imposed by the fundamental principles of constitutive modeling such as those related to the principle of objectivity are not automatically fulfilled and thus, they require special attention. However, thermodynamical principles are most frequently not carefully considered within this modeling class, but the respective traction-separation laws are directly postulated in an ad-hoc manner, cf. [9, 25, 26]. Within the framework of (classical) continuum mechanics, such models would consequently be refereed to as Cauchy-elastic. By way of contrast, thermodynamically consistent cohesive models belonging to the second group of interface approaches can be found in [21–23]. With the sole exception of the work [21], only isotropic[1] models are discussed within the cited paper. As mentioned in [22], this is due to the additional structural tensors required for describing the material's anisotropy. For instance, if a mode-I mode-II-III decomposition is considered, the material's anisotropy can be suitably defined by the normal vector $\boldsymbol{n}$ of the respective crack. However, $\boldsymbol{n}$ changes during deformation and thus, it also leads to a change in Helmholtz energy. Since no energetically conjugate variable has been introduced in [21, 22], this term would lead either to unphysical dissipation (even in case of fully elastic deformations), or the stiffness matrix characterizing the interface would be unsymmetric (even in case of fully elastic deformations). Clearly, both points are not physical. A first attempt towards an anisotropic interface model for the second modeling class was made in [21]. However, a more careful analysis reveals that the aforementioned critical points have not been considered and thus, the resulting model is not thermodynamically consistent.

Recently, a thermodynamically consistent framework suitable for the analysis of a certain class of interfaces was proposed in [29]. Focus was on hyperelastic boundary potentials. For describing anisotropic materials, structural tensors were included within the respective Helmholtz energy. By focusing on hyperelastic solids and by applying the principle of minimum potential energy, the balance equations and the constitutive response were derived. According to [29], additional stress tensors energetically conjugate to the change in the structural tensors naturally occurred. In the present paper, a similar viewpoint is adopted. However, and in sharp contrast to [29], internal interfaces including an irreversible response are analyzed.

Adopting a thermodynamically and energetically consistent viewpoint, the novel class of interface models advocated within the present paper is based on a certain Helmholtz energy. For a broad range of application, only few assumptions are made. More specifically, this energy is additively decomposed into different parts related to the different failure modes (such as mode-I failure). Each failure mode depending on evolving structural tensors, in turn, is governed by an effective scalar-valued damage parameter which is multiplicatively decomposed into the underlying degradation mechanisms. Starting with this Helmholtz energy, the interface models are derived by rigorously applying the Coleman & Noll procedure. The probably most important step within the derivation is the introduction of additional stress tensors within the stress power. Such stresses, similar to those in [29] can be interpreted as stresses related to the deformational surface shear. To the best knowledge of the authors, those stresses which are required for thermodynamical consistency at finite strains, have not been taken into account in

---

[1] In the present paper, cohesive zone models are derived from a Helmhholtz energy Ψ depending, among other variables, on the displacement jump $[\![\boldsymbol{u}]\!]$, i.e., $\Psi = \Psi([\![\boldsymbol{u}]\!])$. In line with a frequently applied notation in continuum mechanics (see [27, 28]), such constitutive models are referred to as *isotropic* in what follows, if the scalar-valued function Ψ depends on $[\![\boldsymbol{u}]\!]$ through its only invariant $||\,[\![\boldsymbol{u}]\!]\,||$. Models not fulfilling this requirement are defined as anisotropic.

existing models yet. Equally importantly, the additional stress tensors can result in an effective traction-separation law showing a non-trivial stress-free configuration consistent with the underlying Helmholtz energy. This configuration is not predicted by conventional, i.e., previous, models. Furthermore, the consideration of the additional stress tensors leads to a unique definition of the controversially discussed fictitious intermediate configuration. More explicitly, traction continuity requires that the interface geometry with respect to the deformed configuration has to be taken as the average of both sides.

Clearly, the constraints imposed by the second law of thermodynamics are relatively weak. Hence, they do not lead to unique evolution equations, but rather to a set of admissible evolution equations. A canonical ordering of this set is given by the principle of maximum dissipation, cf. [30]. Material models obeying that principle are also referred to as *standard dissipative solids*, cf. [31, 32]. It can be shown that maximizing the dissipation is in many cases equivalent to minimizing the stress power, cf. [33, 34]. This equivalence gave rise to the introduction of so-called *variational constitutive updates* as advocated by Ortiz and co-workers [35–37] and further also elaborated by others, see, e.g., [38–42]. Within such updates all unknown state variables, together with the total deformation, follow jointly and conveniently from minimizing the integrated stress power. The mathematically and physically elegant variational structure of those updates results in significant advantages compared to standard conventional approaches. For instance, standard optimization algorithms can be applied for solving the mechanical problem. Furthermore, a minimization principle implies the existence of a natural distance (semi metric) which is the foundation for error estimation and thus, for adaptive finite elements methods, cf. [43]. For the aforementioned reasons, the novel class of interface models is reformulated into that variationally consistent framework. Consequently, the admissible states implied by the new models can be interpreted as stable energy minimizers. This variational structure is also used within the numerical implementation yielding a so-called *variational constitutive update*.

The present paper is organized as follows: First, existing interface models are briefly discussed and analyzed in Section 2. Subsequently, the kinematics induced by localized material failure are concisely reviewed in Section 3. The probably most important novel contributions can be found in Sections 4 and 5. While Section 4 is concerned with fully elastic interfaces, material degradation is considered in Section 5. The mechanical response of the resulting model is first analyzed in Section 6 for a single material point. A more complex numerical example is studied in Section 7.

2   State of the art review – existing models

In this section, the most frequently applied modeling classes suitable for the development of cohesive interface laws are briefly discussed. Only those models which are based on a spatial description will be analyzed. Approaches associated with the material displacement jump can be found elsewhere, e.g., in [4].

In line with the recent work [44], the existing models are classified into potential-based formulations and non-potential-based. However and in contrast to [44], large strain effects will also be considered and special attention is drawn to the thermodynamical consistency.

2.1   Non-potential-based models

Within non-potential-based models, the traction vector $\boldsymbol{T}$ acting within the respective shear band or crack is a priori and in an ad-hoc manner coupled to the displacement jump $[\![\boldsymbol{u}]\!]$, cf., e.g., [9, 25, 26]. As a result, focusing on elastic processes and neglecting material anisotropies for now, such models are of the form

$$\boldsymbol{T} = \boldsymbol{T}([\![\boldsymbol{u}]\!]). \tag{1}$$

Accordingly, they would be referred to as Cauchy-elastic within the framework of continuum mechanics, see [28]. As a result, symmetry of their tangent matrix is not a priori guaranteed and thus, such models cannot be derived from a potential in general. Therefore, the resulting dissipation might be non-vanishing, even in case of elastic loading.

An additional problem associated with this modeling class is that usually two independent models are introduced: one for loading and an additional ad-hoc model for unloading, cf. [45]. This is again in sharp contrast to the thermodynamically sound procedure known from classical stress-strain-based constitutive models. For instance, in case of finite strain plasticity theory (see [46]), loading as well as unloading follow jointly and uniquely from the definition of the same Helmholtz energy. The same holds for damage-type constitutive laws, see [47].

In summary, even though the applicability of non-potential-based models have been shown in many practical applications, these models are not thermodynamically consistent in general. Consequently, it is desirable to improve such models accordingly.

Remark 1 *Some authors claim that due to the path-dependence, the tangent matrix $d\boldsymbol{T}/d\llbracket \boldsymbol{u} \rrbracket$ does not need to be necessarily symmetric, see [48]. Therefore, they abandon the symmetry requirement completely. This statement is, however, only partly correct. First, although symmetry and path-dependence are indeed related, they are not equivalent. More explicitly, path-dependent associative plasticity models do lead to a symmetric tangent. Secondly and even more importantly, interfaces can unload elastically. At least in this case, the respective matrix has to be symmetric.*

2.2 Potential-based models

The previous discussion showed that a thermodynamically sound cohesive models has necessarily to be derived from a potential energy. In this subsection, two different classes of potential-based models are briefly discussed. While, traditional Xu & Needleman-type approaches are addressed in the first paragraph, models based on a stored Helmholtz energy are analyzed subsequently.

2.2.1 Models in line with that of Xu & Needleman, cf. [49, 50]

Within the modeling class originally proposed by Xu & Needleman, cf. [49, 50] (see also [44] and references cited therein), the traction vector is derived from a potential ϕ. More explicitly,

$$\boldsymbol{T} = \frac{\partial \phi}{\partial \llbracket \boldsymbol{u} \rrbracket}, \quad \text{with} \quad \phi = \phi(\llbracket \boldsymbol{u} \rrbracket). \tag{2}$$

Again, referring to stress-strain-based constitutive models, traction-separation law (2) would be called hyperelastic. However, such models are usually applied to the modeling of material failure which is intrinsically a non-conservative process. Equally importantly, the dissipation related to material failure is not defined by this class of material models, at least not explicitly. The third critical point is similar to one of the non-potential-based models. Since Eq. (2), although a potential, is designed for capturing the material response under loading, an additional cohesive model is required in case of unloading. Usually, linear elastic unloading to the origin is assumed. In summary, models in line with Xu & Needleman, cf. [49, 50] do still not solve all problems previously discussed for non-potential-based approaches.

2.2.2 Models based on a stored energy potential

Only relatively recently, thermodynamically consistent cohesive models have been proposed, cf. [21–23]. Analogously to standard stress-strain-relations, their foundation is the assumption of a suitable energy potential. In contrast to Xu & Needleman-type constitutive laws, this energy, which is the Helmholtz energy, depends in addition to the displacement jump also an a set of internal variables related to the deformation history. Starting from this Helmholtz energy, the traction-separation law is derived by applying the Coleman & Noll procedure. It bears emphasis that the resulting constitutive model holds for loading as well as for unloading. In this respect, the framework is unique, i.e, one Helmholtz energy defines all states (provided the deformation and the internal variables are known). For developing suitable evolution equations for the internal variables, the second law of thermodynamics is employed. As a consequence, the constraints imposed by the principles of thermodynamics are a priori fulfilled. For these reasons, only this class of models will be considered in presented paper.

2.3 Finite deformation – spatial description

Finally, some complementary remarks concerning a spatial description are given here. In the case of large deformations, additional principles such as that of objectivity have also to be taken into account. However, the probably most serious point is related to the modeling of material anisotropies (see footnote on page 2) such as that implied by a decomposition of the traction vector into a normal and a shear part. As mentioned in [22], the structural tensors may evolve and consequently, they lead to a change in the Helmholtz energy. For instance, taking the normal vector $\boldsymbol{n}$ of a crack as the structural tensor, focusing on fully elastic processes, together with a stress power of the type $\boldsymbol{T} \cdot \llbracket \dot{\boldsymbol{u}} \rrbracket$, the dissipation reads

$$\mathcal{D} = \boldsymbol{T} \cdot \llbracket \dot{\boldsymbol{u}} \rrbracket - \dot{\Psi}(\llbracket \boldsymbol{u} \rrbracket, \boldsymbol{n}) = \left(\boldsymbol{T} - \partial_{\llbracket \boldsymbol{u} \rrbracket} \Psi \right) \cdot \llbracket \dot{\boldsymbol{u}} \rrbracket - \partial_{\boldsymbol{n}} \Psi \cdot \dot{\boldsymbol{n}} \tag{3}$$

Here, Ψ is the Helmholtz energy. Hence, by postulating the standard relation $\boldsymbol{T} = \partial_{\llbracket \boldsymbol{u} \rrbracket} \Psi$, the dissipation does not vanish. This is the reason why so far only isotropic models being thermodynamically sound can be found in the literature. In the present paper, however, anisotropic models which also fulfill the second law of thermodynamics are derived for the first time.

3 Kinematics of discontinuous deformation mappings

This section is concerned with a concise summary of the kinematics induced by strong discontinuities. Furthermore, it provides the notations used within the present paper. Further details on the kinematics of discontinuous deformation mappings can be found elsewhere, e.g., in [4, 8, 51].

In what follows, a body Ω is considered to be separated during deformation into the two parts Ω^- and Ω^+ by means of an internal surface $\partial_s\Omega$, i.e., $\Omega = \Omega^- \cup \Omega^+ \cup \partial_s\Omega$ (Fig. 1). Physically speaking, $\partial_s\Omega$ is a crack or a shear band. The orientation of $\partial_s\Omega$ with respect to the undeformed configuration is locally defined by its normal vector
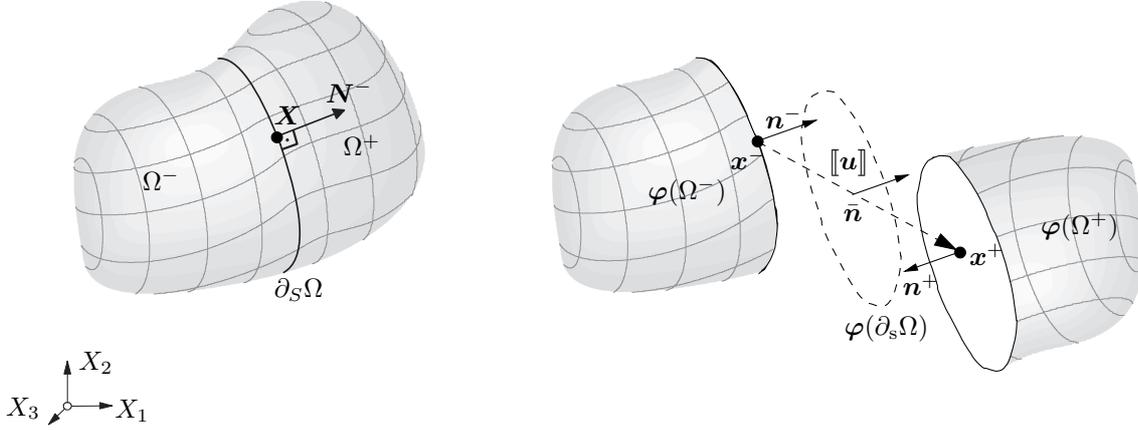

Figure 1: Body $\Omega \subset \mathbb{R}^3$ separated into two parts Ω^- and Ω^+ by an interface $\partial_s\Omega$

N. In line with standard notation, the normal vectors are postulated as pointing outwards, i.e., $N^- = -N^+ = N$. Since the interface $\partial_s\Omega$ is a two-dimensional submanifold in $\mathbb{R}^3$ (at least locally), it proves convenient to represent it by means of curvilinear coordinates θ_α ($\theta = 1; 2$), i.e.,

$$X = X(\theta_\alpha), \quad \forall X \in \partial_s\Omega. \tag{4}$$

With this parameterization, the tangent vectors $G_\alpha = \partial_{\theta_\alpha}X$, the normal vector $N = G_1 \times G_2/||G_1 \times G_2||$ as well as the contravariant basis G^α can be computed in standard manner.

The motion of the sub-bodies Ω^- and Ω^+ is described by the deformation mapping $\varphi : \Omega \ni X \mapsto x \in \varphi(\Omega)$. By introducing the displacement field u, φ can be rewritten as $\varphi = \mathrm{id} + u$ with id being the identity mapping. According to Fig. 1, the undeformed configuration is continuous, while the displacement field is discontinuous. Consequently, denoting $u^\pm$ as the displacement field in Ω^+ and Ω^- and H_s as the Heaviside function of $\partial_s\Omega$, u is of the type

$$u = u^- + H_s \left(u^+ - u^-\right). \tag{5}$$

With Eq. (5) and assuming sufficient regularity of u, the displacement discontinuity $[\![u]\!]$ at $\partial_s\Omega$ can be uniquely defined as

$$[\![u]\!] = u^+ - u^- \quad \forall X \in \partial_s\Omega. \tag{6}$$

As a result, a point X belonging to the interface $\partial_s\Omega$ decomposes during deformation into the two non-connected points

$$\begin{aligned} x^- &= X + u^- \\ x^+ &= X + u^- + [\![u]\!] \end{aligned} \qquad \forall X \in \partial_s\Omega. \tag{7}$$

Since the deformation in Ω^- and that in Ω^+ are in general uncoupled, the normal vectors n^- and n^+ associated with that point are usually not parallel. For this reason, a fictitious intermediate configuration $\bar{x}$ between x^- and x^+ is frequently considered (dashed surface in Fig. 1). Introducing a scalar-valued weighting parameter α, that new configuration can be defined as

$$\bar{x} = (1 - \alpha)\, x^- + \alpha\, x^+, \quad \alpha \in [0; 1]. \tag{8}$$

In most cases, α is set to $\alpha = 1/2$, i.e., the fictitious deformed interface is assumed to be the average of x^- and x^+. Based on x^-, x^+ and $\bar{x}$, the local topology of the deformed interface $\partial_s\Omega$ can be computed in line with that of the undeformed configuration, i.e.,

$$\begin{aligned} g_\alpha^- &= \partial_{\theta_\alpha} x^- & n^- &= g_1^- \times g_2^- / ||g_1^- \times g_2^-|| \\ g_\alpha^+ &= \partial_{\theta_\alpha} x^+ & n^+ &= g_1^+ \times g_2^+ / ||g_1^+ \times g_2^+|| \\ \bar{g}_\alpha &= \partial_{\theta_\alpha} \bar{x} & \bar{n} &= \bar{g} \times \bar{g} \ / \ ||\bar{g} \times \bar{g}||. \end{aligned} \tag{9}$$

The choice of the parameter α defining the normal vector of the intermediate configuration is a controversially discussed subject in the literature, cf. [9, 21, 22, 52]. In the present paper, it will be shown that the condition of traction continuity leads to a uniquely defined parameter α.

4   Elastic Interfaces

This section is concerned with the modeling of interfaces showing a fully elastic response, i.e., focus is on hyperelastic material models fulfilling the second law of thermodynamics. By utilizing the framework of rational thermodynamics (see [19, 20]), all constitutive laws discussed here are rigorously derived by means of the by now classical Coleman & Noll procedure, cf. [53]. Consequently, the dissipation inequality (equality in case of purely elastic deformations)

$$D = \overset{\circ}{w} - \dot{\Psi} = \geq 0 \tag{10}$$

decomposed into the stress power $\overset{\circ}{w}$ and the material time derivative of the Helmholtz energy Ψ will play an important role. Though the procedure originally introduced in [53] is well established in case of standard stress-strain-type constitutive laws, it has not been considered for a general framework of cohesive zone models in a spatial setting yet.

   This section is organized as follows: In Subsection 4.1, isotropic constitutive models are briefly discussed. The extensions necessary for anisotropic materials are given in Subsection 4.2. A special subclass of those being models based on a decomposition of the deformation into a normal component and a shear part is analyzed in Subsection 4.3. Finally, the mechanical response of the novel family of cohesive models is highlighted in Subsection 4.4.

4.1   Isotropic models

Isotropic cohesive models are nowadays relatively well understood, cf. [21–23]. Expressing the Helmholtz energy Ψ in terms of quantities associated with respect to the deformed configuration, Ψ does not depend on any structural tensoris, i.e., Ψ is allowed to depend only on the jump $[\![u]\!]$ itself. Consequently,

$$\Psi = \Psi([\![u]\!]) \quad \Rightarrow \quad \dot{\Psi} = \frac{\partial \Psi}{\partial [\![u]\!]} \cdot \dot{[\![u]\!]}. \tag{11}$$

According to Eq. (11), only one stress-like variable conjugate to $[\![u]\!]$ is present. By denoting this variable, which is the traction vector within the interface, as T, the stress power is written as

$$\overset{\circ}{w} = T \cdot \dot{[\![u]\!]}. \tag{12}$$

Hence, application of the Coleman & Noll procedure yields

$$\mathcal{D} = \left[T - \frac{\partial \Psi}{\partial [\![u]\!]} \right] \cdot \dot{[\![u]\!]} = 0 \quad \Rightarrow \quad T = \frac{\partial \Psi}{\partial [\![u]\!]}. \tag{13}$$

As a result and as expected, the stress vector T is the partial derivative of the Helmholtz energy with respect to its dual variable $[\![u]\!]$.

   For analyzing the mechanical response induced by a Helmholtz energy of the type (11), the restrictions imposed by the principle of material frame indifference ($\Psi([\![u]\!]) = \Psi(Q \cdot [\![u]\!])$, $\forall Q \in SO(3)$) are a priori enforced. As shown, e.g., in [54, 55], they are equivalent to postulating

$$\Psi = \Psi(|| [\![u]\!] ||). \tag{14}$$

Hence, Ψ is allowed to depend on $[\![u]\!]$ only through its only invariant $|| [\![u]\!] ||$. This requirement is equivalent to the standard definition of isotropy of a scalar-valued tensor function (see footnote on page 2). Using Eq. (14), the traction vector $(13)_2$ results in

$$T = \frac{\partial \Psi}{\partial || [\![u]\!] ||} \frac{[\![u]\!]}{|| [\![u]\!] ||}. \tag{15}$$

Accordingly, T is parallel to the displacement discontinuity $[\![u]\!]$. Therefore, such models are frequently interpreted as rubber bands connecting the two different sides of an interface, cf. [9, 22].

4.2 Anisotropic models

In the more general case, the stored energy functional Ψ may additionally depend on some structural tensors a_i. Accordingly, the respective energy reads

$$\Psi = \Psi(\llbracket u \rrbracket, a_1, \ldots a_n). \tag{16}$$

Since a spatial setting is adopted, those tensors may evolve in time, i.e., $\dot{a}_i \neq 0$. They are related to their time-invariant material counterparts A_i by a push-forward transformation. For that purpose, the average deformation gradient

$$\bar{F} = (1 - \alpha)\, F^- + \alpha\, F^+, \qquad \alpha \in [0;1] \tag{17}$$

is introduced. In Eq. (17), $F^{\pm}$ are the surface deformation gradients, cf. [29], i.e., F^+ and F^- map only tangent vectors. Clearly, by using the cross product of such tangent vectors, the normal vector can nevertheless be computed. For $\alpha = 1/2$, $\bar{F}$ results in the classical average deformation gradient. Evidently, the choice of α will affect the resulting traction-separation law. This will be analyzed in Subsection 4.4. By combining Eq. (16) with Eq. (17), the Helmholtz energy (16) can be rewritten as

$$\Psi = \Psi(\llbracket u \rrbracket, F^-, F^+, A_1, \ldots A_n), \quad \text{with} \quad \dot{A}_i = 0. \tag{18}$$

The analogy between cohesive laws and boundary potential energies can clearly be seen from Eq. (18). More precisely, by denoting the deformation gradient characterizing an external boundary as $\hat{F}$ and its normal with respect to the undeformed configuration as N, the respective energies are often assumed to be of the type

$$\Psi = \Psi(\hat{F}, N), \quad \text{with} \quad \dot{N} = 0 \tag{19}$$

(see [29] for a recent overview). Hence, for constant displacement jumps $\llbracket u \rrbracket$ and the special choice $A_1 = N$, the cohesive model (18) can indeed be interpreted as a sum of two boundary potentials. However and in contrast to boundary potentials associated with external surfaces, cohesive models have to fulfill certain compatibility conditions, i.e., traction continuity. It will be shown that the constraints imposed by such conditions will define the parameter α.

Starting from Eq. (18) and assuming further that the spatial vectors a_i are defined by a push-forward of their material counterparts A_i through the deformation gradient (17), the rate of the Helmholtz energy is computed as

$$\dot{\Psi} = \frac{\partial \Psi}{\partial \llbracket u \rrbracket} \cdot \dot{\llbracket u \rrbracket} + \frac{\partial \Psi}{\partial \bar{F}} : \left[(1 - \alpha)\, \dot{F}^- + \alpha\, \dot{F}^+ \right]. \tag{20}$$

It bears emphasis that the deformation gradients $F^{\pm}$ and the displacement discontinuity $\llbracket u \rrbracket$ are only weakly coupled ($F^+ = F^- + \mathrm{GRAD}\,\llbracket u \rrbracket$). Hence, the stress power consists of three terms in general. By introducing two stress tensors $P^{\pm}$ of first Piola-Kirchhoff type being conjugate to the deformation gradients $F^{\pm}$, the stress power can thus be written as

$$\overset{o}{w} = T \cdot \dot{\llbracket u \rrbracket} + P^- : \dot{F}^- + P^+ : \dot{F}^+. \tag{21}$$

Although this decomposition of the stress power is natural, it seems that all existing cohesive models in the literature do not account for the two additional terms related to $F^{\pm}$. Evidently, if the deformation is infinitesimally small, these terms can be neglected. However, for finite strains they do not vanish and consequently, they have to be taken into account. Physically speaking, they correspond to the boundary potentials of each side $\Omega^{\pm}$. Alternatively, the constitutive models addressed in the present paragraph can be interpreted as gradient-type models, since in contrast to $\llbracket u \rrbracket$, $F^{\pm}$ are gradient terms. Independently of the interpretation, the respective terms also appear, if only the normal vector N of the displacement discontinuity is taken as a structural tensor. Consequently, the aforementioned points apply to all models based on a decomposition of the traction vector into a normal component and a shear part. Accordingly, without considering the additional terms in Eq. (21), such models are not thermodynamically consistent and hence, they can result in non-vanishing dissipation even in case of elastic unloading. In Subsection 4.4 this aspect is carefully analyzed by means of an illustrative example.

Having defined the Helmholtz energy and its corresponding rate (20) and having introduced the stress power (21), the constitutive relations are obtained from the by now standard Coleman & Noll procedure, cf. [53], i.e., by evaluating the dissipation inequality for fully reversible states, the constitutive equations

$$T = \frac{\partial \Psi}{\partial \llbracket u \rrbracket}, \quad P^- = \frac{\partial \Psi}{\partial F^-} = (1 - \alpha)\, \frac{\partial \Psi}{\partial \bar{F}}, \quad P^+ = \frac{\partial \Psi}{\partial F^+} = \alpha\, \frac{\partial \Psi}{\partial \bar{F}} \tag{22}$$

are found. Accordingly, in addition to the classical constitutive model $(22)_1$, two boundary-like laws are also implicitly defined by the Helmholtz energy (18). They are formally identical to those reported in [29]. However

and in contrast to boundary potentials, the total stress vector T characterizing cohesive models (internal interfaces) is subjected to the condition of traction continuity. Thus, by considering Cauchy's equation $T = P \cdot N$, the only admissible choice for the scalar-valued parameter α is $\alpha = 1/2$, i.e., the fictitious mid-surface. This is an interesting result, since many discussions on the choice of α can be found in the literature, cf. [9, 21, 22, 52].

It should be noted that besides the condition of traction continuity, the principle of material frame indifference imposes some additional constraints on the Helmholtz energy Ψ, i.e., $\Psi(\llbracket u \rrbracket, a_1, \ldots a_n) = \Psi(Q \cdot \llbracket u \rrbracket, Q \cdot a_1, \ldots, Q \cdot a_n)$, $\forall Q \in SO(3)$ has to hold. As stated in [54, 55], such constraints can be effectively fulfilled by using an irreducible integrity basis. However, since this basis is, depending on the number n, quite lengthy, it is omitted here. In case of $n = 1$ which will be discussed in the next subsection, some further comments on objectivity will be given.

Remark 2 *In the present paper, both the deformation gradient of the bulk as well as that at of an interface are denoted as F. From the authors point of view, confusion is nevertheless excluded. Usually, F is the surface deformation gradient whenever an interface is considered. Otherwise, it will be stated explicitly.*

4.3 Mixed-mode models based on a normal-shear decomposition of the displacement discontinuity

It has been observed in many experimnents that the failure mechanisms in mode-I or mode-II and mode-III can differ significantly, cf. [9]. In the present subsection, a cohesive zone model capturing such features is discussed. For that purpose, a decomposition of the displacement jump and the traction vector into a normal component and the remaining shear part is frequently applied, cf. [21, 44] (see also [9] and references cited therein). Such constitutive laws can be considered as a special case of those discussed in the previous subsection. More explicitly, they correspond to

$$\Psi = \Psi(\llbracket u \rrbracket, F^-, F^+, A_1), \quad \text{with} \quad A_1 = N. \tag{23}$$

Here, N is the normal vector defining locally the topology of the internal surface $\partial_s \Omega$. Since $\bar{n} = \bar{n}(\bar{F}, N)$, application of Eqs. (22) yields

$$T = \frac{\partial \Psi}{\partial \llbracket u \rrbracket} \quad \text{and} \quad \begin{aligned} P^- &= \frac{\partial \Psi}{\partial F^-} = (1 - \alpha) \frac{\partial \Psi}{\partial \bar{F}} = -(1 - \alpha) \, \bar{n} \otimes \frac{\partial \Psi}{\partial \bar{n}} \cdot \bar{F}^{-T} \\ P^+ &= \frac{\partial \Psi}{\partial F^+} = \quad \alpha \frac{\partial \Psi}{\partial \bar{F}} = \quad -\alpha \, \bar{n} \otimes \frac{\partial \Psi}{\partial \bar{n}} \cdot \bar{F}^{-T}. \end{aligned} \tag{24}$$

Within the representation of $P^{\pm}$ as a rank-one tensor, the classical deformation gradient has to be used (more precisely, $n = F^{-T} \cdot N$). For highlighting the analogy between this family of cohesive models and boundary potential energies, Eqs. $(24)_2$ and $(24)_3$ are rewritten as

$$P^- = \bar{n} \otimes \hat{S}_0^-$$
$$P^+ = \bar{n} \otimes \hat{S}_0^+ \tag{25}$$

with

$$\hat{S}_0^- = -(1 - \alpha) \frac{\partial \Psi}{\partial \bar{n}} \cdot \bar{F}^{-T}$$
$$\hat{S}_0^+ = \quad -\alpha \frac{\partial \Psi}{\partial \bar{n}} \cdot \bar{F}^{-T}. \tag{26}$$

Accordingly, $\hat{S}$ can be interpreted as a deformational surface shear, cf. [29, 56]. Furthermore and as already mentioned in the previous subsection, continuity of the traction vector requires $\alpha = 1/2$.

Since the class of cohesive models discussed within the present subsection is frequently applied in solid mechanics, the constraints imposed by the principle of material frame indifference are briefly summarized as well. According to [54, 55], an energy of the type $\Psi = \Psi(\llbracket u \rrbracket, \bar{n})$ is material frame indifferent, if and only if it can be expressed in terms of $\| \llbracket u \rrbracket \|$ and the normal component of the displacement jump $\llbracket u \rrbracket \cdot \bar{n}$. Hence, the Helmholtz energy has to be of the type

$$\Psi = \tilde{\Psi}(\| \llbracket u \rrbracket \|, \bar{u} \cdot \bar{n}). \tag{27}$$

Since the norm of the shear deformation $\llbracket u \rrbracket_s$ can be written as

$$\| \llbracket u \rrbracket_s \| = \sqrt{\| \llbracket u \rrbracket \|^2 - (\llbracket u \rrbracket \cdot \bar{n})^2}, \quad \text{with} \quad \llbracket u \rrbracket_s := \llbracket u \rrbracket - (\llbracket u \rrbracket \cdot \bar{n}) \, \bar{n} \tag{28}$$

every Helmholtz energy of the form $\Psi = \Psi(\llbracket u \rrbracket \cdot \bar{n}, \| \llbracket u \rrbracket_s \|)$ fulfills evidently the principle of material frame indifference (see, e.g., [21, 52]).

a) $\alpha = 0.5$, $\beta = 180°$ b) $\alpha = 1.0$, $\beta = 90°$

Figure 2: Non-trivial stress-free configurations of the interface model (29) for two different parameters α.

4.4 Illustrative example

In this section, the influence of the stress tensors $\boldsymbol{P}^{\pm}$ as well as the choice of the parameter α defining the deformed configuration of the internal surface $\partial_s\Omega$ is carefully analyzed. For that purpose, a mode-I traction-separation law characterized by a Helmholtz energy of the type

$$\Psi = \frac{1}{2}\, c\, (\llbracket \boldsymbol{u} \rrbracket \cdot \bar{\boldsymbol{n}})^2 \tag{29}$$

is considered. Here, c is a material parameter related to the stiffness of the interface. For analyzing the mechanical response corresponding to Helmholtz energy (29), a straight and vertically oriented interface of unit length is chosen (see Fig. 2). Consequently, with $\boldsymbol{e}_i$ denoting the vectors of the cartesian basis, the undeformed configuration is given by

$$\boldsymbol{X} = \boldsymbol{e}_2\, \theta, \qquad \theta \in [0; 1] \tag{30}$$

with θ representing the curvilinear coordinate. This interface is fixed on the left hand side, while the right hand side moves during deformation. Thus, the deformed configuration is described by

$$\boldsymbol{x}^- = \boldsymbol{X}, \qquad \boldsymbol{x}^+ = \boldsymbol{x}^- + \llbracket \boldsymbol{u} \rrbracket, \qquad \bar{\boldsymbol{x}} = (1 - \alpha)\, \boldsymbol{x}^- + \alpha\, \boldsymbol{x}^+. \tag{31}$$

It bears emphasis that the intermediate configuration $(\bar{\bullet})$ enters the potential Ψ only through the normal vector $\bar{\boldsymbol{n}}$. Thus, the length of the interface in the intermediate configuration is irrelevant. Since the influence of $\boldsymbol{P}^{\pm}$ and that of α on the resulting traction vector is only visible in case of large deformations and a non-vanishing gradient of the displacement discontinuity, a displacement field of the type

$$\llbracket \boldsymbol{u} \rrbracket = \llbracket \boldsymbol{u} \rrbracket^{(n)}\, \theta, \quad \text{with} \quad \llbracket \boldsymbol{u} \rrbracket^{(n)} = [\sin\beta; \cos\beta - 1]^T \tag{32}$$

is adopted. In Eq. (32), $\llbracket \boldsymbol{u} \rrbracket^{(n)}$ is the displacement discontinuity at the position $\theta = 1$ of the interface. According to Eqs. (32) and (31), the vertically oriented interface is fixed at the left hand side, while the right hand side is rotated around the position $\theta = 0$ of the interface, cf. Fig. 2. Having defined the deformation of the interface, the tangent vector $\bar{\boldsymbol{g}}_1 = \partial_\theta \bar{\boldsymbol{x}}$ of the fictitious deformed configuration can be computed and finally, the normal vector $\bar{\boldsymbol{n}}$ with $\bar{\boldsymbol{n}} \cdot \bar{\boldsymbol{g}}_1 = 0$ and $||\bar{\boldsymbol{n}}|| = 1$. Clearly, since the interface remains straight during deformation (the deformation depends linearly on θ), the normal vector is spatially constant, i.e., $\bar{\boldsymbol{n}} \neq \bar{\boldsymbol{n}}(\theta)$.

In what follows, the stress vector and the integrated force vector associated with the interface model (29) as a result of the aforementioned deformation mode are analyzed. By applying Eq. (24)$_1$, the linearly varying traction vector implied by Eq. (29) yields

$$\boldsymbol{T} = \partial_{\llbracket \boldsymbol{u} \rrbracket}\Psi = c\, (\llbracket \boldsymbol{u} \rrbracket \cdot \bar{\boldsymbol{n}})\, \bar{\boldsymbol{n}} \tag{33}$$

and thus, the corresponding force is obtained as

$$\boldsymbol{F}_{\boldsymbol{T}} := \int_0^1 \frac{\partial \Psi}{\partial \llbracket \boldsymbol{u} \rrbracket}\, \mathrm{d}\theta = \int_0^1 \boldsymbol{T}\, \mathrm{d}\theta = \frac{1}{2}\, c\, (\llbracket \boldsymbol{u} \rrbracket^{(n)} \cdot \bar{\boldsymbol{n}})\, \bar{\boldsymbol{n}}. \tag{34}$$

Accordingly, $\boldsymbol{T}$ as well as the force vector $\boldsymbol{F}_{\boldsymbol{T}}$ are parallel to $\bar{\boldsymbol{n}}$.

As evident, the considered deformation does not only lead to a monotonically increasing displacement jump $\llbracket \boldsymbol{u} \rrbracket$, but also to a varying normal vector $\bar{\boldsymbol{n}}$. The stresses or forces related to such a variation are included in the

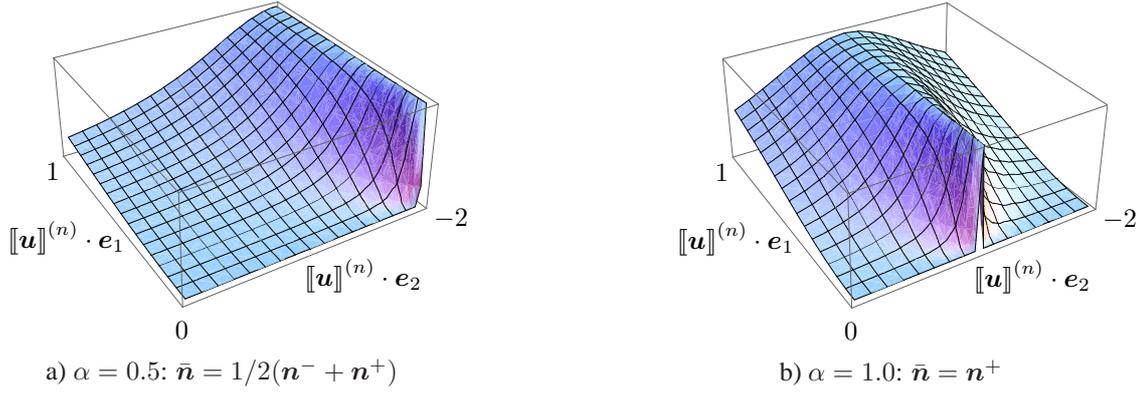a) $\alpha = 0.5$: $\bar{n} = 1/2(n^- + n^+)$ b) $\alpha = 1.0$: $\bar{n} = n^+$

Figure 3: Integrated Helmholtz energy (29) depending on the parameter α as function in terms of the displacement discontinuity $[\![u]\!]$.

stress tensors $P^{\pm}$, cf. Eq. (24). Alternatively, they can be taken into account by replacing the partial derivative in Eq. (34) by the total differential, i.e.,

$$F_{\text{total}} := \int_0^1 T_{\text{total}} \, d\theta := \int_0^1 \frac{d\Psi}{d[\![u]\!]} \, d\theta = \int_0^1 \left[T + \frac{\partial \Psi}{\partial \bar{n}} \cdot \frac{\partial \bar{n}}{\partial [\![u]\!]} \right] d\theta. \tag{35}$$

It bears emphasis that usually F_{total} depends on $F^{\pm}$ as well. However, for the special deformation analyzed here, $[\![u]\!]$ is the only independent displacement-like variable. More precisely, $F^+ = F^- + \text{GRAD}\,[\![u]\!]$, together with $F^- = \text{const}$, holds. As a result, a variation of the Helmholtz energy Ψ with respect to F^+ can equivalently be expressed by a variation of the displacement discontinuity, i.e.,

$$\delta F^+ = \delta\text{GRAD}\,[\![u]\!] = \delta [\![u]\!]^{(n)} \otimes G^1. \tag{36}$$

Here, G^1 is the first covariant vector. Clearly, since G_i is a cartesian basis, $G^1 = G_1 = e_2$ holds. By combining Eq. (36) with Eq. (24)$_3$, the variation of the Helmholtz energy through the normal vector $\bar{n}$ is computed as

$$\begin{aligned} \delta_{\bar{n}} \partial \Psi &:= \frac{\partial \Psi}{\partial \bar{n}} \cdot \frac{\partial \bar{n}}{\partial \bar{F}} : \delta \bar{F} \\ &= \frac{\alpha\, c}{\theta} \left([\![u]\!] \cdot \bar{n} \right) \left([\![u]\!] \cdot \frac{\partial \bar{n}}{\partial \bar{F}} \cdot G^1 \right) \cdot \delta [\![u]\!] \end{aligned} \tag{37}$$

and consequently, the total tractions T_{total} acting within the interface are given by

$$T_{\text{total}} = \underbrace{c\,([\![u]\!]^{(n)} \cdot \bar{n})\,\bar{n}}_{= T} + \underbrace{\frac{\alpha\, c}{\theta}\,([\![u]\!] \cdot \bar{n}) \left([\![u]\!] \cdot \frac{\partial \bar{n}}{\partial \bar{F}} \cdot G^1 \right)}_{:= T_{\bar{n}}}. \tag{38}$$

In Eq. (37), the identity $\delta \bar{F} = \alpha\, \delta F^+$ has been used. Evidently, $T_{\bar{n}}$ is related to a variation of the normal vector.

While the interpretation of T is straightforward, T_{total} can be conveniently analyzed by the integrated Helmholtz energy. For two different parameters α, this energy is shown in Fig. 3. According to Fig. 3b), the energy has a local extremum at $[\![u]\!]^{(n)} \cdot e_2 = -1$ for $\alpha = 1.0$. Consequently, the respective stress vector T_{total} vanishes. At first glance, a non-trivial stress-free configuration seems to be unphysical. However, that state corresponds to a rotation of Ω^+ of $\beta = 90°$. As shown in Fig. 2b), in this case, a variation of $[\![u]\!]^{(n)} \cdot e_1$ does not influence the normal component $[\![u]\!] \cdot n$ and therefore, the energy should indeed be constant in X_1-direction. Furthermore, a straightforward computations shows that the energy is symmetric with respect to a variation of $[\![u]\!]^{(n)} \cdot e_2$ for $\beta = 90°$. For this reason, this non-trivial stress-free configuration is indeed consistent with the underlying Helmholtz energy. It bears emphasis that this physically relevant configuration is captured by none of the existing models. Fortunately, it only appears, if the rotation between both sides of the interface is very large and thus, it can often be neglected in practical applications. Furthermore, it depends crucially on the underlying constitutive law as well as on the parameter α.

5   Inelastic interfaces – Damage models

Having discussed the fully reversible case, focus is now on inelastic processes. In the present section, theses processes are assumed to be associated with stiffness degradation of the considered interface. Hence, they will be modeled by means of damage mechanics. For plastic effects, the interested reader is referred to [16, 17].

This section is structured as follows: First, the fundamentals of the novel family of damage models are given in Subsection 5.1. In Subsection 5.2, two prototype models falling into the range of that family are briefly summarized: an isotropic as well as a mixed-mode fracture model. The novel constitutive description is completed by suitable damage evolutions which are summarized in Subsection 5.3. Having introduced the new framework for interface models, a variationally consistent reformulation is elaborated in Subsection 5.4. The section finishes with some remarks concerning the numerical implementation (Subsection 5.5).

5.1   Fundamentals

In this section, a class of damage models is presented. For broadening the range of application, only few assumptions are made. The first of those is the additive decomposition of the interface's elastic energy into different modes, i.e.,

$$\Psi^{\mathrm{e}} = \sum_{i=1}^{n} \Psi_i(\llbracket \boldsymbol{u} \rrbracket, \boldsymbol{F}^+, \boldsymbol{F}^-). \tag{39}$$

Each Helmholtz energy Ψ_i possibly depending on structural tensors is associated with one characteristic deformation mode. A typical example is given in Subsection 5.2.2, where the energy is decomposed into a shear part and an additional contribution corresponding to the normal separation. A similar decomposition is also frequently applied in standard stress-strain-based constitutive models, cf. [57, 58]. The second assumption is that material damage can be suitably approximated by means of a set of scalar-valued damage parameters. However, since each deformation type i is captured by its own damage variable, this assumption is not very crucial and provides enough flexibility. Furthermore, scalar-valued damage parameters lead to an effective numerical implementation. The final assumption is that the different damage mechanisms are coupled multiplicatively. Accordingly, the total Helmholtz energy of the respective interface reads

$$\Psi = \sum_{i=1}^{n} \prod_{j=1}^{n} (1 - d_i^{(j)}) \, \Psi_i(\llbracket \boldsymbol{u} \rrbracket, \boldsymbol{F}^+, \boldsymbol{F}^-). \tag{40}$$

Evidently, postulating the standard properties of the damage variables $d_i^{(j)} \in [0; 1]$ automatically guarantees that the effective damage variable is bounded accordingly, i.e.,

$$(1 - d_i^{\mathrm{eff}}) := \prod_{j=1}^{n} (1 - d_i^{(j)}) \quad \Rightarrow \quad d_i^{\mathrm{eff}} \in [0; 1]. \tag{41}$$

This would not be the case for an additive decomposition. Application of the Coleman & Noll procedure yields the stress response

$$\boldsymbol{T} = \sum_{i=1}^{n} \prod_{j=1}^{n} (1 - d_i^{(j)}) \, \frac{\partial \Psi_i}{\partial \llbracket \boldsymbol{u} \rrbracket} \qquad \begin{aligned} \boldsymbol{P}^- &= (1 - \alpha) \sum_{i=1}^{n} \prod_{j=1}^{n} (1 - d_i^{(j)}) \, \frac{\partial \Psi_i}{\partial \bar{\boldsymbol{F}}} \\ \boldsymbol{P}^+ &= \alpha \sum_{i=1}^{n} \prod_{j=1}^{n} (1 - d_i^{(j)}) \, \frac{\partial \Psi_i}{\partial \bar{\boldsymbol{F}}}, \end{aligned} \tag{42}$$

cf. Eq. (24), together with the reduced dissipation inequality

$$\mathcal{D} = \mathring{w} - \dot{\Psi} = \sum_{i=1}^{n} \sum_{j=1}^{n} \prod_{k=1, k \neq j}^{n} (1 - d_i^{(k)}) \, \Psi_i(\llbracket \boldsymbol{u} \rrbracket, \boldsymbol{F}^+, \boldsymbol{F}^-) \, \dot{d}_i^{(j)} \geq 0. \tag{43}$$

Since the elastic energies Ψ_i are assumed to be non-negative and $d_i^{(j)} \in [0; 1]$, the second law of thermodynamics is automatically fulfilled, if $d_i^{(j)}$ is monotonically increasing, i.e.,

$$\dot{d}_i^{(j)} \geq 0. \tag{44}$$

Clearly, physically speaking, Ineq. (44) avoids self-healing of the material.

The class of models presented here is completed by deriving evolution equations fulfilling $\dot{d}_i^{(j)} \geq 0$. For that purpose, a suitable set of internal variables has to be introduced. Conceptually, one could use $d_i^{(j)}$ directly. However, by doing so, it might be difficult to enforce the boundedness $d_i^{(j)} \in [0;1]$. Therefore, a rescaling by means of internal variables $\kappa_i^{(j)} \in [0;\infty)$ is considered, i.e., $d_i^{(j)}$ is assumed to be of the type $d_i^{(j)} = d_i^{(j)}(\kappa_i^{(j)})$. As a result, by defining the internal variables $\kappa_i^{(j)}$ as well as $d_i^{(j)}$ as monotonically increasing, all physical constraints are fulfilled.

By analyzing the reduced dissipation inequality (43), different choices for the internal variables $\kappa_i^{(j)}$ can be motivated. The two probably most obvious choices are

$$d_i^{(j)} = d_i^{(j)}(\kappa_i^{(j)}), \quad \kappa_i^{(j)} = \Psi_i \tag{45}$$

and

$$d_i^{(j)} = d_i^{(j)}(\kappa_i^{(j)}), \quad \kappa_i^{(j)} = \prod_{k=1, k \neq j}^{n} (1 - d_i^{(k)})\, \Psi_i. \tag{46}$$

Clearly, the constraints $\dot{\kappa}_i^{(j)} \geq 0$ have to be enforced additionally. In case of Eq. (45), only n internal variables being the elastic energies associated with the different deformation modes are required, while Eq. (46) seems to result in twice as many variables. However, a careful analysis of Eq. (46) reveals that also in that case, the different failure modes are uncoupled, i.e., by inserting some of the equations into others one can show that $\kappa_i^{(j)} = \kappa_i^{(j)}(\Psi_i)$. Therefore, the choices (45) and (46) are essentially identical.

Eq. (46) would imply that the failure modes are uncoupled. However, experimental observations do not confirm such a response in general. A typical example is given by a crack, where mode-I crack opening leads to a reduction of the shear stiffness as well. For taking such a coupling into account and inspired by Eq. (45), n internal variables of the type

$$\kappa_i(t_{n+1}) = \max\{\kappa_i(t_n); \Psi_i(t_{n+1})\}, \qquad \kappa_i(t = 0) = \kappa_{i(0)} \tag{47}$$

are chosen. Here, $t_{n+1} > t_n$ denote two pseudo time steps. According to Eq. (47), the irreversibility constraints $\dot{\kappa}_i \geq 0$ have already been accounted for. In contrast to Eq. (45), the interactions between different failure modes are included by a damage evolution of the type

$$d_i^{(j)} = d_i^{(j)}(\kappa_j). \tag{48}$$

It should be noticed that the indices in Eq. (48) are flipped compared to Eq. (45). The features of the resulting class of damage models are explained next by considering two prototype models.

5.2   Examples

5.2.1   Isotropic models

The first prototype model is the well known isotropic damage model, cf. [21–23]. It is based on a Helmholtz energy of the type

$$\Psi = (1 - d)\, \Psi^{\mathrm{e}}([\![\boldsymbol{u}]\!]) \tag{49}$$

where the elastic part Ψ^{e} depends only on the norm of the displacement discontinuity, cf. Subsection 4.1. Often the simplest choice being possible

$$\Psi^{\mathrm{e}} = \frac{1}{2}\, c\, ||\, [\![\boldsymbol{u}]\!]\, ||^2 \tag{50}$$

is made. Based on Eq. (49) the thermodynamical driving force conjugate to d is chosen as the elastic stored energy, i.e.,

$$d = d(\kappa), \quad \kappa(t_{n+1}) = \max\{\kappa(t_n); \Psi^{\mathrm{e}}(t_{n+1})\}, \quad \kappa(t_0) = \kappa_0. \tag{51}$$

5.2.2   Mixed-mode models based on a normal-shear decomposition of the displacement discontinuity

Next, a more realistic model based on a decomposition of the failure mode into a normal separation and a shear deformation is shown. Referring to the general framework elaborated in Subsection 5.1, it corresponds to $n = 2$. While the first part of the Helmholtz energy Ψ_{n} is related to mode-I failure, Ψ_{s} is associated with a mode-II and mode-III deformation. Accordingly, a Helmholtz energy of the type

$$\Psi = (1 - d_{\mathrm{n}}^{(\mathrm{n})})\,(1 - d_{\mathrm{n}}^{(\mathrm{s})})\,\Psi_{\mathrm{n}} + (1 - d_{\mathrm{s}}^{(\mathrm{n})})\,(1 - d_{\mathrm{s}}^{(\mathrm{s})})\,\Psi_{\mathrm{s}} \tag{52}$$

is considered and the elastic energies Ψ_n and Ψ_s have the form

$$\Psi_n = \Psi_n([\![\boldsymbol{u}]\!] \cdot \bar{\boldsymbol{n}}), \quad \Psi_s = \Psi_s(|| [\![\boldsymbol{u}]\!]_s ||). \tag{53}$$

Evidently, they fulfill automatically the conditions imposed by the principle of material frame indifference, cf. Subsection 4.3. For the examples presented in Sections 6 and 7, the quadratic energies

$$\Psi_n([\![\boldsymbol{u}]\!] \cdot \bar{\boldsymbol{n}}) = \frac{1}{2} c_n ([\![\boldsymbol{u}]\!] \cdot \bar{\boldsymbol{n}})^2, \quad \Psi_s = \Psi_s(|| [\![\boldsymbol{u}]\!]_s ||) = \frac{1}{2} c_s || [\![\boldsymbol{u}]\!]_s ||^2 \tag{54}$$

are adopted. The model is completed by suitable evolution equations. In line with the previous subsection, they are taken as

$$d_i^{(j)} = d_i^{(j)}(\kappa_j), \quad \kappa_j(t_{n+1}) = \max\{\kappa_j(t_n); \Psi_j(t_{n+1})\}, \quad \kappa_j(t_0) = \kappa_{j0}. \tag{55}$$

It bears emphasis that this model fulfills all physically relevant properties and additionally those recently postulated in [44]. The probably most important two similarities are listed below:

- Complete failure occurs, if one of the critical separations (energies) is reached:
  Let κ_j^{crit} denote the critical stored energy of mode j. At this stage, a stress-free macroscopic cracks forms. By designing the damage functions $d_i^{(j)}$ such that $d_i^{(j)}(\kappa_j) \to 1$ for $\kappa_j \to \kappa_j^{\text{crit}}$, the stored energy converges automatically to zero as well. Consequently, $\boldsymbol{T} = \boldsymbol{0}$, if $\kappa_j \to \kappa_j^{\text{crit}}$.

- Symmetry and anti-symmetry conditions of the traction vector:
  Let $[\![\boldsymbol{u}]\!] = [\![\boldsymbol{u}]\!]_n + [\![\boldsymbol{u}]\!]_s$ and $\boldsymbol{T} = \boldsymbol{T}_n + \boldsymbol{T}_s$ be the decompositions of the displacement jump and the traction vector into the normal and the shear part. Since $\Psi_n = \Psi_n([\![\boldsymbol{u}]\!]_n)$, $\Psi_s = \Psi_s(|| [\![\boldsymbol{u}]\!]_s ||)$ and $\boldsymbol{T}$ depends linearly on $[\![\boldsymbol{u}]\!]$, it follows trivially that $\boldsymbol{T}_n([\![\boldsymbol{u}]\!]_n, [\![\boldsymbol{u}]\!]_s) = \boldsymbol{T}_n([\![\boldsymbol{u}]\!]_n, -[\![\boldsymbol{u}]\!]_s)$ and $\boldsymbol{T}_s([\![\boldsymbol{u}]\!]_n, [\![\boldsymbol{u}]\!]_s) = -\boldsymbol{T}_n([\![\boldsymbol{u}]\!]_n, -[\![\boldsymbol{u}]\!]_s)$.

5.3 Damage evolution

To complete the family of damage models introduced before, suitable evolution equations for the damage variables $d_i^{(j)} = d_i^{(j)}(\kappa_j)$ are required. Since these equations are, with the sole exception of the respective material parameters, identical for all damage variables, indices are omitted in what follows, i.e., without loss of generality, $d = d(\kappa)$ will be considered. Evidently, the choice of $d = d(\kappa)$ will influence the shape of the resulting traction-separation law and consequently, it can affect the overall structural response, cf. [7, 59]. For this reason, three different models $d = d(\kappa)$ have been implemented:

- Linear softening

$$d = \begin{cases} 0 & \kappa < \kappa_{\text{nucl}} \\ 1 - \dfrac{\kappa_{\text{nucl}}}{\kappa}\left(\dfrac{\kappa_{\text{ini}} - \kappa}{\kappa_{\text{ini}} - \kappa_{\text{nucl}}}\right) & \kappa_{\text{nucl}} < \kappa < \kappa_{\text{ini}} \\ 1 & \kappa_{\text{ini}} < \kappa \end{cases} \tag{56}$$

- Power-law hardening/softening

$$d = \begin{cases} 0 & \kappa < \kappa_{\text{nucl}} \\ 1 - \left(\dfrac{\kappa_{\text{ini}} - \kappa}{\kappa_{\text{ini}} - \kappa_{\text{nucl}}}\right)^n & \kappa_{\text{nucl}} < \kappa < \kappa_{\text{ini}} \\ 1 & \kappa_{\text{ini}} < \kappa \end{cases} \tag{57}$$

- Softening involving a stress plateau

$$d = \begin{cases} 0 & \kappa < \kappa_{\text{nucl}} \\ 1 - \dfrac{T_0}{c\kappa} & \kappa_{\text{nucl}} < \kappa < \kappa_2 \\ 1 + \dfrac{T_0}{c\kappa_2}\left(\dfrac{1 - \kappa/\kappa_{\text{ini}}}{1 - \kappa_2/\kappa_{\text{ini}}}\right)^2 \left[\dfrac{\kappa}{\kappa_2} + 2\dfrac{1 - \kappa/\kappa_{\text{ini}}}{1 - \kappa_2/\kappa_{\text{ini}}} - 4\right] & \kappa_2 < \kappa < \kappa_{\text{ini}} \\ 1 & \kappa_{\text{ini}} < \kappa \end{cases} \tag{58}$$

Here, κ_{nucl} and κ_{ini} are the thresholds of the internal variable κ associated with crack nucleation and initiation of a macrocrack, respectively. Furthermore, n is a material parameter. The C^1-continuous damage evolution (58) has been designed such that a constant cohesive traction of magnitude T_0 is obtained within the interval $[\kappa_{\text{nucl}} = T_0/c; \kappa_2 = k_2\kappa_{\text{ini}}]$ (e.g. with $k_2 = 0.5$). The different damage evolutions (56)–(58), together with the equivalent stress-displacement responses, are summarized in Fig. 4.
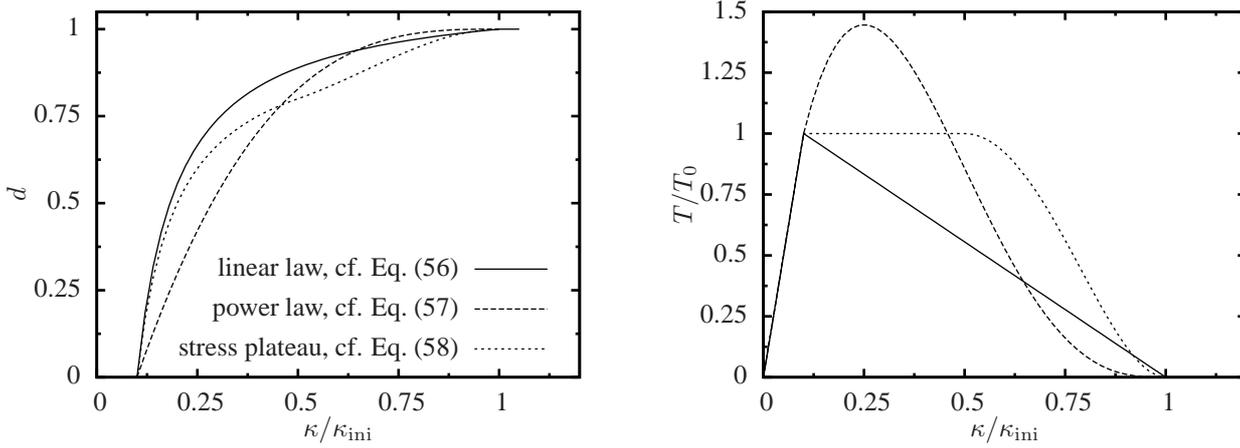
Figure 4: Left: various damage evolution laws defined in Eqs. (56)-(58); right: resulting traction-separation laws (material parameters: $\kappa_{\mathrm{nucl}} = 0.1$, κ_{ini}, $n = 3$, $\kappa_2 = 0.5\ \kappa_{\mathrm{ini}}$; κ is chosen as the maximum displacement discontinuity, cf. Remark 3)

Remark 3 *In contrast to the previous section and in line with most cohesive models, the equivalent displacement discontinuity implied by the elastic energies is chosen as the internal variable. For instance instead of the energy $\Psi = 1/2\ c\ ||\llbracket u \rrbracket||^2$, $||\llbracket u \rrbracket||$ is considered directly. However, since $\sqrt{\Psi} = \sqrt{2/c}\ ||\llbracket u \rrbracket||$, both choices are essentially equivalent.*

5.4 The variational structure of damage models

Within the previous subsections, a family of cohesive models applicable to the analysis of a broad range of different materials, including those showing a pronounced anisotropic response, has been elaborated. In sharp contrast to other interface models based on a geometrically exact description, the proposed constitutive framework is thermodynamically consistent, i.e., the second law of thermodynamics is fulfilled.

Following [30], a canonical ordering of thermodynamically consistent models is provided by the principle of maximum dissipation. In many cases, this principle is equivalent to minimizing the stress power, cf. [33, 34]. This alternative formulation can be conveniently discretized by a suitable time integration yielding effective so-called *variational constitutive updates* as advocated by Ortiz and co-workers [35–37], see also [38–42]. Within such updates all unknown state variables, together with the total deformation, follow jointly and conveniently from minimizing the integrated stress power. The resulting mathematical and physical advantages are manifold compared to standard conventional approaches, cf. [34].

In the present subsection, the proposed class of cohesive material models will be reformulated within the aforementioned variational framework, i.e., the advocated class of constitutive laws can be characterized by the optimization problem

$$\inf \mathcal{E} \qquad \text{with} \qquad \mathcal{E} = \dot{\Psi} + \mathcal{D}. \tag{59}$$

Here, $\mathcal{E}$ is the stress power which can be decomposed into the rate of the Helmholtz energy Ψ and the dissipation $\mathcal{D}$. It bears emphasis that although variational constitutive updates were already introduced for standard stress-strain-type constitutive models a decade ago (see [35–37]), they have not been considered for cohesive models yet.

5.4.1 Isotropic models

For the isotropic models according to Subsection 5.2.1, the equivalence between the already discussed constitutive framework and a variational principle of the type (59) can be shown in a relatively straightforward manner. For that purpose, the dissipation

$$\mathcal{D} = \Psi^{\mathrm{e}}\ \frac{\partial d}{\partial \kappa}\ \dot{\kappa} = \kappa\ \frac{\partial d}{\partial \kappa}\ \dot{\kappa} \geq 0 \tag{60}$$

is inserted into the stress power

$$\mathcal{E} = \frac{\partial \Psi}{\partial \llbracket u \rrbracket} \cdot \llbracket \dot{u} \rrbracket - \frac{\partial \Psi}{\partial d}\ \frac{\partial d}{\partial \kappa}\ \dot{\kappa} + \kappa\ \frac{\partial d}{\partial \kappa}\ \dot{\kappa} = T \cdot \llbracket \dot{u} \rrbracket - (\Psi^{\mathrm{e}} - \kappa)\ \frac{\partial d}{\partial \kappa}\ \dot{\kappa}. \tag{61}$$

It is important to note that Eq. (60) is fulfilled for loading ($\Psi = \kappa$) as well as for unloading ($\dot{\kappa} = 0$). Hence, the second term in Eq. (61) vanishes always and thus,

$$\mathcal{E} = \boldsymbol{T} \cdot [\![\dot{\boldsymbol{u}}]\!] \tag{62}$$

is indeed the stress power. Furthermore and equally importantly, a minimization of $\mathcal{E}$ with respect to the internal variable $\dot{\kappa}$ gives the evolution equation and the loading conditions. More explicitly,

$$\inf_{\dot{\kappa}} \mathcal{E}|_{[\![\dot{\boldsymbol{u}}]\!]=\mathrm{const}} \quad \Leftrightarrow \quad \kappa \geq \Psi^{\mathrm{e}}. \tag{63}$$

As a result, minimization principle (63) leads eventually to

$$\kappa(t_{n+1}) = \max\{\kappa(t_n); \Psi^{\mathrm{e}}(t_{n+1})\} \tag{64}$$

which is equivalent to the evolution equation (51) postulated in Subsection 5.2.1.

Having minimized $\mathcal{E} = \mathcal{E}([\![\dot{\boldsymbol{u}}]\!], \dot{\kappa})$ with respect to the internal variables $\dot{\kappa}$ gives rise to the introduction of the reduced stress power

$$\tilde{\mathcal{E}}([\![\dot{\boldsymbol{u}}]\!]) = \inf_{\dot{\kappa}} \varepsilon([\![\dot{\boldsymbol{u}}]\!], \dot{\kappa}). \tag{65}$$

Evidently, $\tilde{\mathcal{E}}$ acts as a hyperelastic stored energy potential defining the traction vector, i.e., $\boldsymbol{T} = \partial_{[\![\dot{\boldsymbol{u}}]\!]} \tilde{\mathcal{E}}$.

5.4.2 Mixed-mode models based on a normal-shear decomposition of the displacement discontinuity

For showing the variational structure of the mixed-mode model as discussed in Subsection 5.2.2, a staggered method is used, i.e., stability of the stress power $\mathcal{E}$ with respect to one active internal variable is analyzed first. Without loss of generality, an active normal mode is considered here. A straightforward computation yields the dissipation

$$\mathcal{D} = \left[\left(1 - d_{\mathrm{n}}^{(\mathrm{s})}\right) \kappa_{\mathrm{n}} \frac{\partial d_{\mathrm{n}}^{(\mathrm{n})}}{\partial \kappa_{\mathrm{n}}} + \left(1 - d_{\mathrm{s}}^{(\mathrm{s})}\right) \Psi_{\mathrm{s}} \frac{\partial d_{\mathrm{s}}^{(\mathrm{n})}}{\partial \kappa_{\mathrm{n}}} \right] \dot{\kappa}_{\mathrm{n}} \geq 0 \tag{66}$$

and thus, the respective stress power reads

$$\mathcal{E} = \dot{\Psi}\Big|_{\dot{\kappa}_{\mathrm{n}}=0} + \left(1 - d_{\mathrm{n}}^{(\mathrm{s})}\right) \frac{\partial d_{\mathrm{n}}^{(\mathrm{n})}}{\partial \kappa_{\mathrm{n}}} \left(\kappa_{\mathrm{n}} - \Psi_{\mathrm{n}}\right) \dot{\kappa}_{\mathrm{n}} \geq 0. \tag{67}$$

Accordingly and in line with the isotropic damage model investigated before, the evolution of the internal variable κ_{n} follows again from the variational principle

$$\inf_{\dot{\kappa}_{\mathrm{n}}} \mathcal{E}\Big|_{[\![\dot{\boldsymbol{u}}]\!]=\mathrm{const}, \dot{\boldsymbol{F}}=\mathrm{const}} \quad \Leftrightarrow \quad \kappa_{\mathrm{n}} \geq \Psi_{\mathrm{n}}. \tag{68}$$

Consequently, the internal variable κ_{n} at time t_{n+1} as predicted by the minimization principle results in

$$\kappa_{\mathrm{n}}(t_{n+1}) = \max\{\kappa_{\mathrm{n}}(t_n); \Psi_{\mathrm{n}}(t_{n+1})\} \tag{69}$$

which is identical to the model presented in Subsection 5.2.2. Evidently, the derivation (66)–(69) can also be applied to the shear mode.

Having considered the case of one active deformation mode, attention is now drawn to the coupled case. For checking whether the other failure mode is also active, stability of the stress power which has already been minimized with respect to the first mode (see Eq. (68)) is analyzed concerning the remanding mode. Considering $\kappa_{\mathrm{n}} = \Psi_{\mathrm{n}}$ (active normal failure), together with $\dot{\kappa}_{\mathrm{s}} = \dot{\Psi}_{\mathrm{s}}$ within the dissipation, yields

$$\mathcal{E} = \dot{\Psi}\Big|_{\dot{\kappa}_{\mathrm{n}}=0} + \left(1 - d_{\mathrm{s}}^{(\mathrm{s})}\right) \frac{\partial d_{\mathrm{s}}^{(\mathrm{n})}}{\partial \kappa_{\mathrm{n}}} \left(\kappa_{\mathrm{s}} - \Psi_{\mathrm{s}}\right) \dot{\kappa}_{\mathrm{n}} + \left(1 - d_{\mathrm{s}}^{(\mathrm{n})}\right) \frac{\partial d_{\mathrm{s}}^{(\mathrm{s})}}{\partial \kappa_{\mathrm{s}}} \left(\kappa_{\mathrm{s}} - \Psi_{\mathrm{s}}\right) \dot{\kappa}_{\mathrm{s}} \geq 0. \tag{70}$$

Accordingly, energy stability with respect to $\dot{\kappa}_{\mathrm{s}}$ requires thus

$$\kappa_{\mathrm{s}} \geq \Psi_{\mathrm{s}}. \tag{71}$$

By comparing Ineq. (71) to Ineq. (68)$_2$ it is evident that activity of a failure mode can be checked by ignoring the other completely. This is a direct consequence of the uncoupling of $\dot{\kappa}_{\mathrm{n}}$ and $\dot{\kappa}_{\mathrm{s}}$ within the stress power. For this reason, a straightforward simultaneous minimization of $\mathcal{E}$ in case of both failure modes being active leads again to

$$\kappa_{\mathrm{n}} \geq \Psi_{\mathrm{n}}, \quad \text{and} \quad \kappa_{\mathrm{s}} \geq \Psi_{\mathrm{s}}. \tag{72}$$

Clearly, this uncoupling is numerically very appealing, since it reduces the complexity of the optimization problem.

Independently of which failure mode is active, a minimization of the stress power with respect to the internal variables κ_{n} and κ_{s} defines a reduced stress power

$$\tilde{\mathcal{E}}(\llbracket \dot{\boldsymbol{u}} \rrbracket, \dot{\boldsymbol{F}}) = \inf_{\dot{\kappa}_{\mathrm{n}}, \dot{\kappa}_{\mathrm{s}}} \mathcal{E}(\llbracket \dot{\boldsymbol{u}} \rrbracket, \dot{\boldsymbol{F}}, \dot{\kappa}_{\mathrm{n}}, \dot{\kappa}_{\mathrm{s}}) \tag{73}$$

which acts like a hypererlastic potential defining the stresses with the interface, i.e.,

$$\boldsymbol{T} = \partial_{\llbracket \boldsymbol{u} \rrbracket} \tilde{\mathcal{E}}, \quad \boldsymbol{P}^{+} = \alpha \, \partial_{\dot{\boldsymbol{F}}} \tilde{\mathcal{E}}, \quad \boldsymbol{P}^{-} = (1 - \alpha) \, \partial_{\dot{\boldsymbol{F}}} \tilde{\mathcal{E}} \tag{74}$$

Remark 4 *The model discussed in this paragraph represents a special case (two failure modes) of the more general class of anisotropic interface laws as introduced in Subsection 5.1. Since this more general class leads also to an uncoupling of the rates of the internal variables κ_i within the stress power, this class can also be reformulated within a variationally consistent format. Since this would require the application of the same technique as employed within the present paragraph (successively), further details are omitted here.*

5.5 Implementational aspects

A standard or conventional implementation of the models described in Subsection 5.1 is straightforward. For that purpose and in line with standard damage theory formulated in strain space (strain-stress-type models), the internal variables κ_i at (pseudo) time t_{n+1} can be directly computed in closed form as

$$\kappa_i(t_{n+1}) = \max \left\{ \kappa_i(t_n); \Psi_i(t_{n+1}) \right\}. \tag{75}$$

Subsequently, the stress vector $\boldsymbol{T}$ and the stress tensors $\boldsymbol{P}^{\pm}$ are determined by Eqs. (42).

Alternatively, the variational principle discussed within the previous subsection can be employed. For that purpose, the continuous problem (59) is transformed into a discrete counterpart by considering the finite time interval $[t_n; t_{n+1}]$, i.e., problem (59) is rewritten as

$$\inf I_{\mathrm{inc}}^{\partial_s \Omega}, \quad I_{\mathrm{inc}}^{\partial_s \Omega} := \int_{t_n}^{t_{n+1}} \mathcal{E} \, \mathrm{d}t = \Psi(t_{n+1}) - \Psi(t_n) + \int_{t_n}^{t_{n+1}} \mathcal{D} \, \mathrm{d}t. \tag{76}$$

For instance, in case of the isotropic model presented in Subsection 5.4.1, $I_{\mathrm{inc}}^{\partial_s \Omega}$ can be computed analytically yielding

$$I_{\mathrm{inc}}^{\partial_s \Omega} = \Psi(t_{n+1}) - \Psi(t_n) + \kappa \, d|_{t_n}^{t_{n+1}} - \int_{\kappa_n}^{\kappa_{n+1}} d \, \mathrm{d}\kappa. \tag{77}$$

Thus, stability of this energy with respect to the unknown internal variable κ at time t_{n+1} requires

$$\begin{aligned}
\frac{\partial I_{\mathrm{inc}}^{\partial_s \Omega}}{\partial \kappa_{n+1}} &= -\Psi^{\mathrm{e}}(t_{n+1}) \frac{\partial d_{n+1}}{\partial \kappa_{n+1}} + d_{n+1} + \kappa_{n+1} \frac{\partial d_{n+1}}{\partial \kappa_{n+1}} - d_{n+1} \\
&= -\left(\Psi^{\mathrm{e}}(t_{n+1}) - \kappa_{n+1}\right) \frac{\partial d_{n+1}}{\partial \kappa_{n+1}} \geq 0.
\end{aligned} \tag{78}$$

Accordingly, the minimization principle $\inf I_{\mathrm{inc}}^{\partial_s \Omega}$ includes the evolution equation

$$\kappa_{n+1} \geq \Psi^{\mathrm{e}}(t_{n+1}) \tag{79}$$

consistently.

The case of a single internal variable κ is very appealing, since the integral (77) can be computed analytically. If more failure mechanisms are considered, the dissipation has to be integrated numerically, e.g., by applying a backward-Euler integration. However, such methods are nowadays standard and therefore, they will not be presented in detail here. Clearly, if the time integration is consistent, consistency of the resulting numerical scheme is guaranteed. As a summary, even if a numerical approximation of the integral is used, the resulting algorithmic formulation of the class of interface models is given by the variational principle

$$(\kappa_1(t_{n+1}), \ldots, \kappa_n(t_{n+1})) = \arg \inf I_{\mathrm{inc}}^{\partial_s \Omega}(\llbracket \boldsymbol{u} \rrbracket_{n+1}, \bar{\boldsymbol{F}}_{n+1}, \kappa_1(t_{n+1}), \ldots, \kappa_n(t_{n+1}))\Big|_{\boldsymbol{\varphi} = \mathrm{const}}. \tag{80}$$

Independently of the number of internal variables, the variational constitutive updates give therefore rise to the reduced functional

$$\tilde{I}_{\mathrm{inc}}^{\partial_s \Omega} = \inf_{\{\kappa_i\}} I_{\mathrm{inc}}^{\partial_s \Omega}. \tag{81}$$

Assuming an analogous variational structure also for the bulk's material model, the functional $\tilde{I}_{\text{inc}}^{\Omega} = \tilde{I}_{\text{inc}}^{\Omega}(\boldsymbol{\varphi})$ is introduced. With these notations, the total energy (work) of the considered structure is given by

$$I_{\text{total}} = I_{\text{total}}(\boldsymbol{\varphi}) = \int_{\Omega} \tilde{I}_{\text{inc}}^{\Omega} \, dV - I_{\text{ext}} + \int_{\partial_{\text{s}}\Omega} \tilde{I}_{\text{inc}}^{\partial_{\text{s}}\Omega} \, dA \tag{82}$$

where the potential I_{ext} is associated with external forces. Accordingly and in line with the local constitutive description, the global boundary value problem is also characterized by a potential structure (which is incrementally defined). More importantly, a minimization of this potential results in the classical equilibrium conditions in weak form, i.e.,

$$\delta I_{\text{total}} = 0 = \int_{\Omega} \boldsymbol{P} : \delta \boldsymbol{F} \, dV - \frac{\partial I_{\text{ext}}}{\partial \boldsymbol{\varphi}} \cdot \delta \boldsymbol{u} + \int_{\partial_{\text{s}}\Omega} \left[\boldsymbol{T} \cdot \delta \llbracket \boldsymbol{u} \rrbracket + \boldsymbol{P}^{\pm} : \delta \boldsymbol{F}^{\pm} \right] \, dA, \; \forall \delta \boldsymbol{u} \tag{83}$$

Here, Eqs. (42), together with $\boldsymbol{P} := \partial_{\boldsymbol{F}} \tilde{I}_{\text{inc}}^{\Omega}$, have been inserted. As evident, the term $\partial I_{\text{ext}}/\partial \boldsymbol{\varphi}$ is a generalized force. Eq. (83) can be conveniently discretized by finite elements. For that purpose, the volume-type integrals are discretized in standard fashion, while the surface integrals are approximated by shell-type elements, i.e., similar to the approach presented in [52]. This is precisely the numerical implementation which has been chosen. The linearization of Eq. (83) necessary for a Newton-type iteration scheme can be computed in standard manner. For that purpose, the stationarity condition defining the constitutive update is linearized, i.e.,

$$\text{d} \left(\inf_{\kappa_i} I_{\text{inc}}^{\partial_{\text{s}}\Omega}|_{\boldsymbol{\varphi}=\text{const}} \right) = 0, \quad \Rightarrow \quad \text{d}\kappa_i = \text{d}\kappa_i(\text{d} \llbracket \boldsymbol{u} \rrbracket, \text{d}\boldsymbol{F}^{\pm}) \tag{84}$$

which, in turn, is inserted into the linearization of Eq. (83). Further details are omitted here and will be discussed in detail in a forthcoming paper. It bears emphasis that due to the underlying variational structure, symmetry of the resulting stiffness matrix is a priori guaranteed, cf. [60].

Remark 5 *By applying the divergence theorem, Eq. (83) can be rewritten as*

$$\begin{aligned} \delta I_{\text{total}} = & -\int_{\Omega} DIV\boldsymbol{P} \cdot \delta \boldsymbol{u} \, dV + \int_{\partial\Omega} \boldsymbol{T} \cdot \delta \boldsymbol{u} \, dA - \delta I_{\text{ext}} \\ & + \int_{\partial_{\text{s}}\Omega} \left(\boldsymbol{T}^- - \boldsymbol{T}_{\text{s}} \right) \cdot \delta \boldsymbol{u} \, dA + \int_{\partial_{\text{s}}\Omega} \left(-\boldsymbol{T}^+ + \boldsymbol{T}_{\text{s}} \right) \cdot \delta \boldsymbol{u} \, dA \\ & + \int_{\partial_{\text{s}}\Omega} \boldsymbol{P}^{\pm} : \delta \boldsymbol{F}^{\pm} \, dA = 0, \; \forall \delta \boldsymbol{u}. \end{aligned} \tag{85}$$

For avoiding confusion between the stress vectors acting at Ω^+, Ω^- and that within the discontinuity surface, the definition $\boldsymbol{T}_{\text{s}} := \partial_{\llbracket \boldsymbol{u} \rrbracket} \tilde{I}_{\text{inc}}^{\partial_{\text{s}}\Omega}$ has been introduced here. According to Eq. (85), the corresponding Euler equations include, among others, the strong from of traction continuity (equilibrium), i.e., $\boldsymbol{T}_{\text{s}} = \boldsymbol{T}^+ = \boldsymbol{T}^-$. With this equilibrium condition, Eq. (85) can be recast into (see Eq. (82))

$$\begin{aligned} \delta \left. I_{\text{total}} \right|_{\delta \llbracket \boldsymbol{u} \rrbracket = \boldsymbol{0}} = & \int_{\Omega} \delta \tilde{I}_{\text{inc}}^{\Omega} \, dV - \delta I_{\text{ext}} \\ & + \int_{\partial_{\text{s}}\Omega} \delta \left. \tilde{I}_{\text{inc}}^{\partial_{\text{s}}\Omega} \right|_{\llbracket \boldsymbol{u} \rrbracket = \text{const}, \boldsymbol{F}^+ = \text{const}} dA \\ & + \int_{\partial_{\text{s}}\Omega} \delta \left. \tilde{I}_{\text{inc}}^{\partial_{\text{s}}\Omega} \right|_{\llbracket \boldsymbol{u} \rrbracket = \text{const}, \boldsymbol{F}^- = \text{const}} dA = 0 \; \forall \delta \boldsymbol{u}. \end{aligned} \tag{86}$$

Consequently, the reduced stationarity problem is formally identical to that of a continuum with two external surface potentials. As a result, the remaining Euler equations are formally identical to those reported given for external boundary potentials, cf. [29].

6   Analysis of the work of separation

In this section, the mechanical response as predicted by the novel class of cohesive models is carefully analyzed. For that purpose, the prototype discussed in Subsection 5.2.2 is considered. Accordingly, the model is based on a

mode-I fracture energy:	200 J/m^2
mode-II/III fracture energy:	100 J/m^2
ultimate stress for mode-I:	3 MPa
ultimate stress for mode-II/III:	12 MPa

Table 1: Fracture energies and ultimate stresses used within the numerical analyses

normal-shear-decomposition of the failure mode. For the sake of comparison, the results obtained from the models proposed in [44] and [61] are also discussed. Within all computations, the fracture energies and the ultimate stresses as summarized in Tab. 1 are used. Furthermore, a linear softening evolution for the pure failure modes (see Eq. (56)) and a power-law softening for the mixed-mode interaction (see Eq. (57)) are considered. For the sake of completeness, the material parameters of the models are given in the appendix (see Tabs. 3-5).

For comparing the different models and in line with [44], the work of separation in normal direction W_n, in tangential direction W_t and the resulting total work W_{tot} are computed according to

$$
\begin{aligned}
W_n &= \int_0^{\delta_{ini}^n} T_n \, d\,[\![u]\!]_n \\
W_t &= \int_0^{\delta_{ini}^t} T_t \, d\,[\![u]\!]_t \\
W_{tot} &= W_n + W_t.
\end{aligned}
\tag{87}
$$

It bears emphasis that the mechanical problems analyzed in this section and originally proposed in [44] are based on a spatially constant displacement jump, i.e., both sides of the crack remain parallel to one another during deformation. Consequently, the normal vector n remains constant as well and as a result, the respective energetically conjugate additional stresses $P^\pm$ vanish.

6.1 Proportional loading

For analyzing proportional loading, the displacement jump is linearly varied. More specifically and focusing on a two-dimensional setting, a displacement jump of the type

$$
\begin{aligned}
[\![u]\!]_n &= \kappa_{ini} \, \sin(\vartheta) t/t_{max} \\
[\![u]\!]_t &= \kappa_{ini} \, \cos(\vartheta) t/t_{max}
\end{aligned}
\tag{88}
$$

is considered. Here t, denotes the current time, $t_{max} \geq t$ is the final time, ϑ denotes an angle allowing to investigate different failure modes and κ_{ini} is the amplitude of the displacement discontinuity at which total material failure occurs.

The work of separation as computed by means of the different models is shown in Fig. 5. According to this figure, all models lead to physically sound results for the limiting cases mode-II ($\vartheta = 0°$) and mode-I ($\vartheta = 90°$), i.e., the computed works of separation equal the respective fracture energies, cf. Tab. 1. Furthermore, the transition between such limiting cases is smooth. Additionally, in [44] it was stated that the total work W_{tot} should be monotonous for a varying failure mode. As can be seen in Fig. 5, this is fulfilled for the model advocated in [44] as well as for the novel constitutive law as elaborated in the present paper. By way of contrast, the model discussed in [61] does not comply with the aforementioned postulate. However, it should be noted that this postulate is not a physical principle. Furthermore, it can also be fulfilled by the damage law in [61] by using a different set of material parameters.

6.2 Non-proportional loading

Next and in line with [44], a non-proportional separation path is investigated, i.e., the interface is first loaded in normal direction until $[\![u]\!]_n = [\![u]\!]_n^1$, and subsequently, the tangential separation is increased up to total failure. The predicted works of separation are summarized in Fig. 6. As in the case of monotonic loading, the limiting cases (mode-I and mode-II failure) are consistently captured by all models and the transition in between is smooth and monotonous.

In summary, the mechanical response as predicted by the novel model is in good agreement with that corresponding to the recently published cohesive law [44]. However, it bears emphasis that only the new model is thermodynamically consistent – even in case of large deformation.
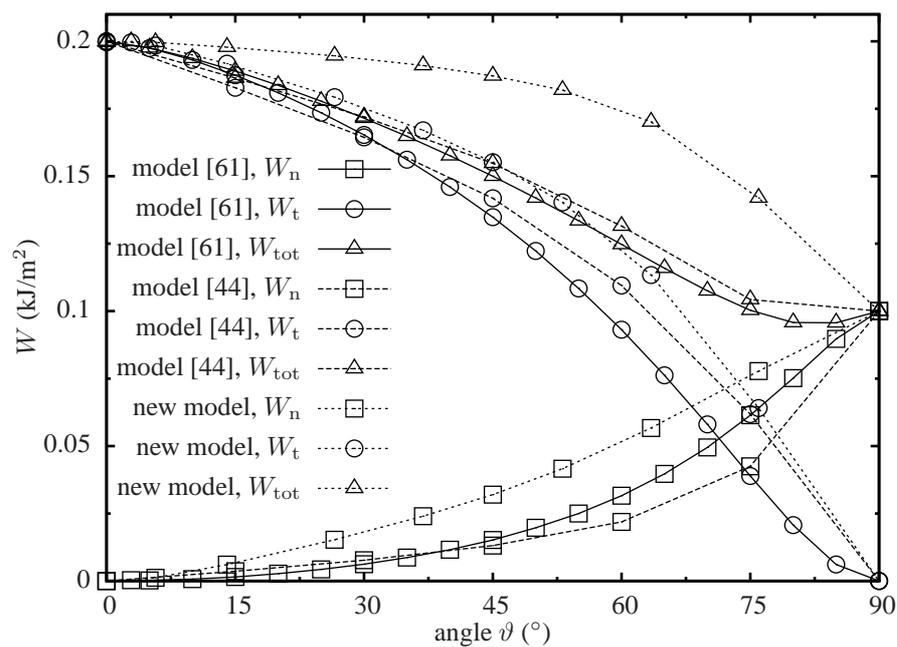
Figure 5: Work of separation as computed by means of different cohesive zone models for a single element under proportional loading (see Eq. (88)).
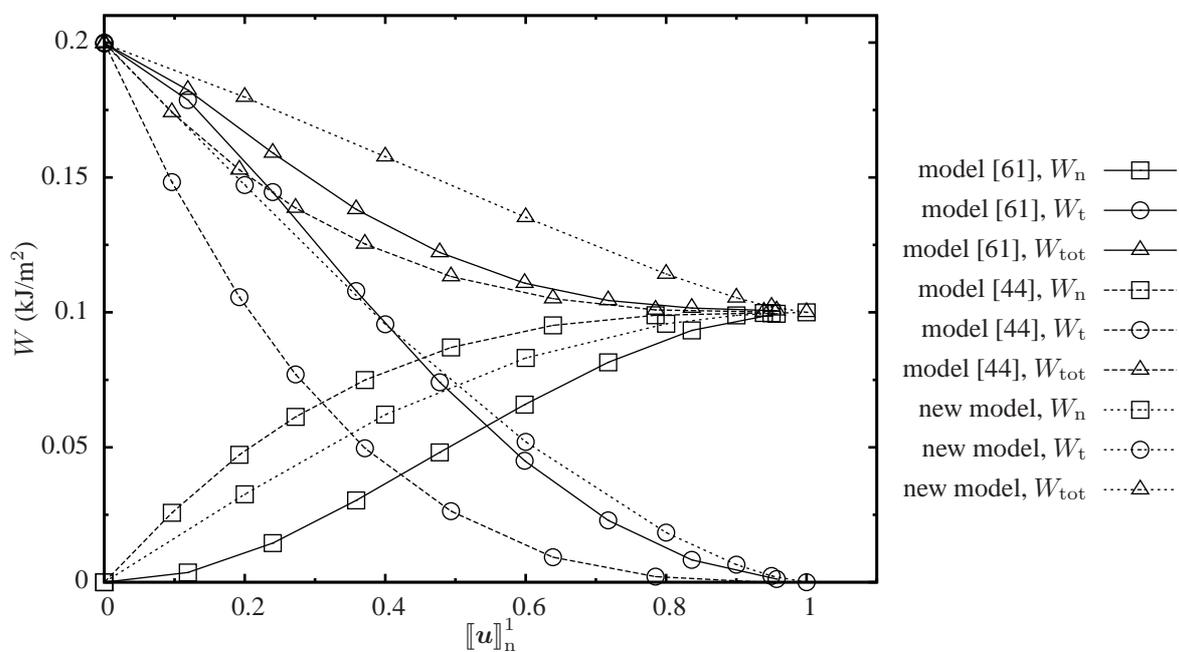

Figure 6: Work of separation as computed by means different cohesive zone models for a single element under non-proportional loading.

7 Numerical example: Double cantilever beam

Finally, the novel interface model is analyzed by means of the more complex boundary value problems shown in Fig. 7. The same precracked specimens have already been studied earlier using other cohesive zone models, cf.
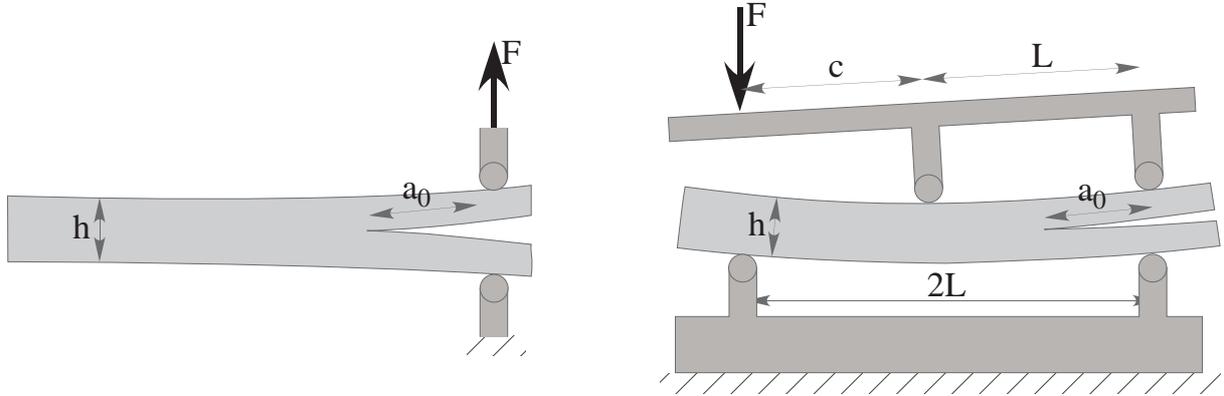

Figure 7: Test specimens for numerical validation of the proposed model; a) double cantilever beam (DCB) specimen for pure mode-I failure; b) mixed-mode bending (MMB) for mixed-mode failure.

[62]. While the geometry is identical within both mechanical problems, the boundary conditions are changed such that the resulting failure is of mode-I within the test shown on the left hand side in Fig. 7 (the so-called *double cantilever beam* (DCB)) and of mixed-mode for the problem depicted on the right hand side in Fig. 7 (the so-called *mixed-mode bending* (MMB) test). The latter was also investigated in [44]. However, the respective parameters are different. Within all computations the mixed-mode model as described in Subsection 5.2.2 has been employed. Again, a linear softening evolution for the pure failure modes (see Eq. (56)) and a power-law softening for the mixed-mode interaction (see Eq. (57)) are considered.

First, the influence of various damage evolution laws on the resulting structural response is investigated. For that purpose the DCB test, together with the evolution equations discussed in Subsection (5.3), is considered (see Fig. 8 (left)). The mode-I ultimate strength of the material and the respective fracture energy have been taken from [62]: $T_{0,\mathrm{n}} = 5.7$ MPa and $\Gamma_{0,\mathrm{n}} = W_{\mathrm{n}}(\llbracket\boldsymbol{u}\rrbracket_{\mathrm{t}} = 0) = 0.28$ kJ/m^2. With these values, the linear softening evolution is uniquely defined. Since this is a pure mode-I problem, the remaining softening evolutions are irrelevant. The results of the computations are summarized in Fig. 8 (right). Accordingly, the effect of the damage evolution is only minor for the analyzed problem.

Next, the effect of the mixed-mode interaction is carefully analyzed by considering the mixed-mode bending beam (MMB). In addition to the mechanical response under mode-I, the mode-II and mixed-mode behavior has also to be defined. The assumed material parameters are summarized in Tab. 2. The results corresponding to

Model	$T_{0,\mathrm{n}}$	$T_{0,\mathrm{t}}$	κ_{nucl}	n
Isotropic (Subsection 5.2.1), var 1	20 MPa		n.a.	n.a.
Isotropic (Subsection 5.2.1), var 2	10 MPa		n.a.	n.a.
Mixed-mode (Subsection 5.2.2), var1	20 MPa	10 MPa	0.99	0.25
Mixed-mode (Subsection 5.2.2), var2	20 MPa	10 MPa	0.25	0.25
Mixed-mode (Subsection 5.2.2), var3	20 MPa	10 MPa	0.25	3

Table 2: Different sets of material parameters used within the numerical analysis of the DCB specimen (see Fig. 7 (left)). Within all sets, the fracture energies are set to $\Gamma_{0,\mathrm{n}} = \Gamma_{0,\mathrm{t}} = 4$ kJ/m^2. The power-law softening for the mixed-mode interaction (see Eq. (57)) is defined by κ_{nucl}, n and $\kappa_{\mathrm{ini}} = 2\,\kappa_{\mathrm{nucl}}$.

the different material models and material parameters in terms of force vs. crack mouth opening displacement (CMOD) are shown in Fig. 9. According to this figure, the ultimate strength of the material does not affect the structural response significantly for an isotropic model. By way of contrast, the interaction between the different failure modes shows a very pronounced effect. While neglecting the interaction completely leads to an ultimate load of over 300 N, a strong interaction ($n = 3$) reduces this ultimate load below 200 N. Therefore, this mechanical problem is well suited for calibrating the material parameters associated with the failure mode interaction.

The example has been re-analyzed without considering the additional membrane-like stresses $\boldsymbol{P}^{\pm}$, i.e., the respective model is thermodynamically inconsistent and does not fulfill the second law of thermodynamics. The
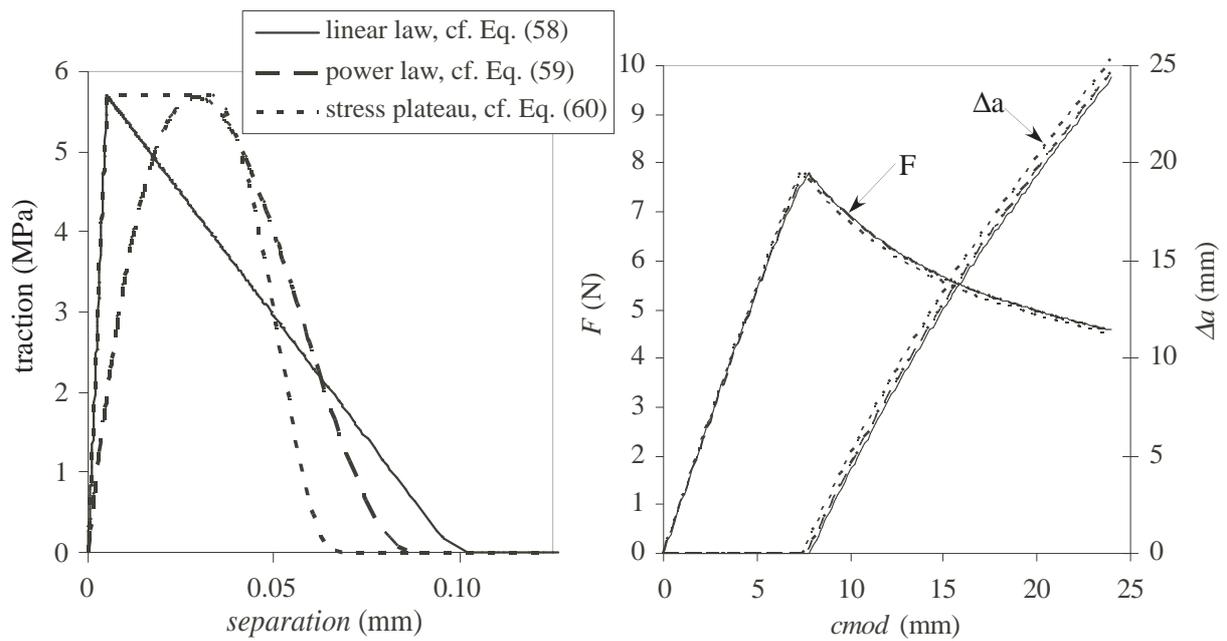
Figure 8: Results of the DCB simulation (see Fig. 7 (left)) with three different damage evolution laws. Left: equivalent traction-separation laws corresponding to the different damage evolutions; Right: force (F) and crack propagation (Δa) depending on the crack mouth opening displacement (cmod).
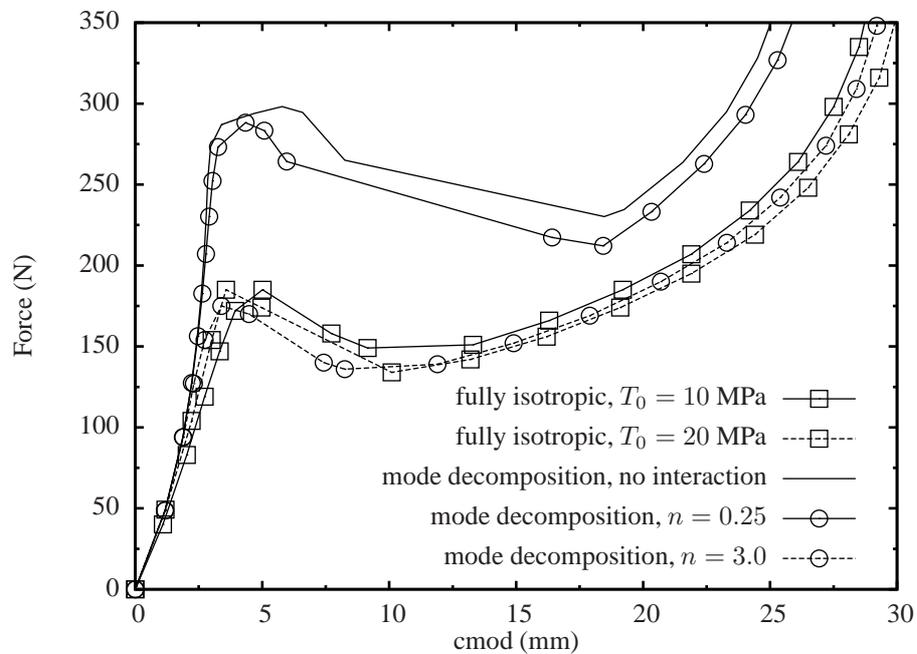

Figure 9: Results of the MMB simulation (see Fig. 7 (right)) using the isotropic model (Subsection 5.2.1) and the mixed-mode model (Subsection 5.2.2) for different sets of material parameters (see Tab. 2).

results of the respective numerical computations are not presented here, since the difference to the original model is very small (approximately, 2 N (1%) in the computed forces). Although such a good agreement depends strongly on the underlying Helmholtz energy and cannot be guaranteed in general (see Subsection 4.4), this result raises hope that the thermodynamical inconsistency of ad-hoc models can be comparably small.

8   Conclusions

In the present paper, a novel class of anisotropic cohesive constitutive models considering large deformation has been presented. In sharp contrast to previously published formulations, all models belonging to the advocated class are thermodynamically consistent, i.e., they were rigorously derived by applying the Coleman & Noll procedure. The probably most interesting new finding from this procedure is the striking analogy between cohesive models and boundary potential energies. This analogy gave rise to the introduction of additional stress tensors which can be interpreted as deformational surface shear. To the best knowledge of the authors, those stresses which are required for thermodynamical consistency at finite strains, have not been taken into account in existing models yet. Accordingly, previous anisotropic cohesive constitutive models considering large deformations are not thermodynamically consistent, i.e., they can result in non-vanishing dissipation even in case of elastic unloading. Fortunately, this thermodynamical inconsistency of ad-hoc models can be comparably small for realistic mechanical systems. However, there is no guarantee for this. For instance, by analyzing a simple mode-I-type cohesive model, it was shown that the aforementioned boundary-like additional stress tensors can result in a traction-separation law showing a non-trivial stress-free configuration consistent with the underlying Helmholtz energy. Such a configuration is not predicted by previous, models. Furthermore, the analogy between cohesive models and boundary potential energies led to a unique definition of the controversially discussed fictitious intermediate configuration, i.e., traction continuity requires that the interface geometry with respect to the deformed configuration has to be taken as the average of both both sides. The novel class of cohesive models was finally reformulated into a variationally consistent framework. More precisely, it was shown the states implied by the novel model can be interpreted as stable energy minimizers. This variational structure was used for deriving a variationally consistent numerical implementation.

A   Material parameters used within the numerical examples presented in Section 6

c_n	c_t	$T_{0,\mathrm{n}}$	$T_{0,\mathrm{t}}$	
4500 MPa/mm	36000 MPa/mm	3 MPa	12 MPa	
$\kappa_{\mathrm{n,ini}} = \kappa_{\mathrm{t,ini}}^{n}$	$\kappa_{\mathrm{t,ini}} = \kappa_{\mathrm{n,ini}}^{t}$	$\kappa_{\mathrm{t,nucl}}^{n} = \kappa_{\mathrm{n,nucl}}^{t}$	$\kappa_{\mathrm{n,nucl}}^{n} = \kappa_{\mathrm{t,nucl}}^{t}$	n
0.0667 mm	0.0333 mm	$0.25\kappa_{\mathrm{t,ini}}$	$0.05\kappa_{\mathrm{n,ini}}$	1.5

Table 3: Material parameters of the new model proposed in the present paper used for the analysis of work of separation under proportional and non-proportional loading
.

Φ_n	Φ_t	$\sigma_{\max}$	$\tau_{\max}$	α	β	λ_n	λ_t
200 J/m^2	100 J/m^2	3 MPa	12 MPa	3	3	0.01	0.01

Table 4: Material parameters of the model proposed by Park, Paulino & Roesler [44] used for the analysis of work of separation under proportional and non-proportional loading.

a_n	a_t	α	γ_n	γ_t	c_n	c_t
49.7 mm/N	25.8 mm/N	2.174	0.105	0.0999	129.5 MPa/mm	1041.4 MPa/mm

Table 5: Material parameters of the model proposed by Allix & Corigliano [61] used for the analysis of work of separation under proportional and non-proportional loading.

References

[1] G.I. Barenblatt. The mathematical theory of equilibrium cracks in brittle fracture. *Adv. Appl. Mech.*, 7:55–129, 1962.

[2] A. Hillerborg, M. Modeer, and P.E. Petersson. Analysis of crack formation and crack growth in concrete by means of fracture mechanics and finite elements. *Cement and Concrete Research*, 6:773–782, 1976.

[3] D.S. Dugdale. Yielding of steel sheets containing slits. *Journal of the Mechanics and Physics of Solids*, 8:100–108, 1960.

[4] J. Mosler. *On the numerical modeling of localized material failure at finite strains by means of variational mesh adaption and cohesive elements*. Habilitation, Ruhr University Bochum, Germany, 2007.

[5] G.A. Francfort and J.-J. Marigo. Revisiting brittle fracture as an energy minimization problem. *Journal of the Mechanics and Physics of Solids*, 46(8):1319–1342, 1998.

[6] A. Chambolle, G.A. Francfort, and J.-J. Marigo. When and how do cracks propagate? *Journal of the Mechanics and Physics of Solids*, 57:1614–1622, 2009.

[7] W. Brocks, A. Cornec, and I. Scheider. *Comprehensive Structural Integrity. Fracture of Materials from Nano to Macro, volume 3*, chapter 03, pages 127–209. Elsevier, Oxford, 2003.

[8] J. Mosler. On the modeling of highly localized deformations induced by material failure: The strong discontinuity approach. *Archives of Computational Methods in Engineering*, 11(4):389–446, 2004.

[9] M.J. van den Bosch, Schreurs P.J.G., and M.G.D. Geers. Identification and characterization of delamination in polymer coated metal sheet. *Journal of the Mechanics and Physics of Solids*, 56:3259–3276, 2008.

[10] K. Garikipati. *On strong discontinuities in inelastic solids and their numerical simulation*. PhD thesis, Stanford University, 1996.

[11] F. Armero and K. Garikipati. An analysis of strong discontinuities in multiplicative finite strain plasticity and their relation with the numerical simulation of strain localization in solids. *International Journal for Solids and Structures*, 33:2863–2885, 1996.

[12] P. Steinmann, R. Larsson, and K. Runesson. On the localization properties of multiplicative hyperelasto-plastic continua with strong discontinuities. *International Journal for Solids and Structures*, 34:969–990, 1997.

[13] R. Larsson, P. Steinmann, and K. Runesson. Finite element embedded localization band for finite strain plasticity based on a regularized strong discontinuity. *Mechanics of Cohesive-Frictional Materials*, 4:171–194, 1998.

[14] R.I. Borja. Finite element simulation of strain localization with large deformation: capturing strong discontinuity using a Petrov-Galerkin multiscale formulation. *Computer Methods in Applied Mechanics and Engineering*, 191:2949–2978, 2002.

[15] J. Mosler. Modeling strong discontinuities at finite strains - a novel numerical implementation. *Computer Methods in Applied Mechanics and Engineering*, 195(33-36):4396–4419, 2006.

[16] M. Fagerström and R. Larsson. Theory and numerics for finite deformation fracture modelling using strong discontinuities. *International Journal for Numerical Methods in Engineering*, 66(6):911–948, 2006.

[17] M. Fagerström and R. Larsson. A thermo-mechanical cohesive zone formulation for ductile fracture. *Journal of Mechanics and Physics of Solids*, 56(10):3037–3058, 2008.

[18] M. Fagerström and R. Larsson. Approaches to dynamic fracture modelling at finite deformations. *Journal of the Mechanics and Physics of Solids*, 56(2):613–639, 2008.

[19] B.D. Coleman and W. Noll. The thermodynamics of elastic materials with heat conduction and viscosity. *Arch. Rational Mech. Anal.*, 13:167178, 1963.

[20] B.D. Coleman. Thermodynamics of materials with memory. *Arch. Rational Mech. Anal.*, 17:1–45, 1964.

[21] Th.C. Gasser and G.A. Holzapfel. Geometrically non-linear and consistently linearized embedded strong discontinuity models for 3D problems with an application to the dissection analysis of soft biological tissues. *Computer Methods in Applied Mechanics and Engineering*, 192:5059–5098, 2003.

[22] J. Mergheim and P. Steinmann. A geometrically nonlinear fe approach for the simulation of strong and weak discontinuities. *Computer Methods in Applied Mechanics and Engineering*, 195:5037–5052, 2006.

[23] R. Radulović and J. Mosler. Effective 3d failure simulations by combining the advantages of embedded strong discontinuity approaches and classical interface elements. *Engineering Fracture Mechanics*, 2010. submitted.

[24] L. Stanković and J. Mosler. Efficient modeling of slip bands by means of a variationally consistent embedded strong discontinuity approach. *International Journal for Numerical Methods in Engineering*, 2010. submitted.

[25] A. Cornec, I. Scheider, and K.-H. Schwalbe. On the practical application of the cohesive model. *Engineering Fracture Mechanics*, 70:1963–1987, 2003.

[26] I. Scheider and W. Brocks. Simulation of cup-cone fracture using the cohesive model. *Engineering Fracture Mechanics*, 70:1943–1961, 2003.

[27] C. Truesdell and W. Noll. The nonlinear field theories. In S. Flügge, editor, *Handbuch der Physik*, volume 3. Springer-Verlag, Berlin, 1965.

[28] J.E. Marsden and T.J.R. Hughes. *Mathematical foundation of elasticity*. Dover, New York, 1994.

[29] P. Steinmann. On boundary potential energies in deformational and configurational mechanics. *Journal of the Mechanics and Physics of Solids*, 56(3):772–800, 2008.

[30] R. Hill. *The mathematical theory of plasticity*. Oxford University Press, Oxford, U.K., 1950.

[31] B. Halphen and Q.S. Nguyen. Sur les matériaux standards généralisés. *Journal de Méchanique*, 14:39–63, 1975.

[32] K. Hackl. Generalized standard media and variational principles in classical and finite strain elastoplasticity. *Journal of the Mechanics and Physics of Solids*, 45(5):667–688, 1997.

[33] K. Hackl and F.D. Fischer. On the relation between the principle of maximum dissipation and inelastic evolution given by dissipation potentials. *Proceedings of the Royal Society A: Mathematical, Physical and Engineering Science*, 464:117–132, 2008.

[34] J. Mosler. Variationally consistent modeling of finite strain plasticity theory with non-linear kinematic hardening. *Computer Methods in Applied Mechanics and Engineering*, 2010. in press.

[35] M. Ortiz and L. Stainier. The variational formulation of viscoplastic constitutive updates. *Computer Methods in Applied Mechanics and Engineering*, 171:419–444, 1999.

[36] M. Ortiz and E.A. Repetto. Nonconvex energy minimisation and dislocation in ductile single crystals. *Journal of the Mechanics and Physics of Solids*, 47:397–462, 1999.

[37] R. Radovitzky and M. Ortiz. Error estimation and adaptive meshing in strongly nonlinear dynamic problems. *Computer Methods in Applied Mechanics and Engineering*, 172:203–240, 1999.

[38] C. Miehe. Strain-driven homogenization of inelastic microstructures and composites based on an incremental variational formulation. *International Journal for Numerical Methods in Engineering*, 55:1285–1322, 2002.

[39] C. Carstensen, K. Hackl, and A. Mielke. Non-convex potentials and microstructures in finite-strain plasticity. *Proceedings of the Royal Society A: Mathematical, Physical and Engineering Science*, 458:299–317, 2002.

[40] E. Fancello, J.-P. Ponthot, and L. Stainier. A variational formulation of constitutive models and updates in non-linear finite viscoelasticity. *International Journal for Numerical Methods in Engineering*, 65:1831–1864, 2006. in press.

[41] J. Mosler and O.T. Bruhns. Towards variational constitutive updates for non-associative plasticity models at finite strain: models based on a volumetric-deviatoric split. *International Journal of Solids and Structures*, 46(7-8):1676–1684, 2009.

[42] J. Mosler and O.T. Bruhns. On the implementation of rate-independent standard dissipative solids at finite strain – Variational constitutive updates. *Computer Methods in Applied Mechanics and Engineering*, 199:417–429, 2010.

[43] J. Mosler and M. Ortiz. Variational h-adaption in finite deformation elasticity and plasticity. *International Journal for Numerical Methods in Engineering*, 72(5):505–523, 2007.

[44] K. Park, G.H. Paulino, and J.R. Roesler. A unified potential-based cohesive model of mixed-mode fracture. *Journal of the Mechanics and Physics of Solids*, 57:891–908, 2009.

[45] M.J. van den Bosch, P.J.G. Schreurs, and M.G.D. Geers. A cohesive zone model with a large displacement formulation accounting for interfacial fibrilation. *European Journal of Mechanics A/Solids*, 26:119, 2007.

[46] J.C. Simo. Numerical analysis of classical plasticity. In P.G. Ciarlet and J.J. Lions, editors, *Handbook for numerical analysis*, volume IV. Elsevier, Amsterdam, 1998.

[47] J.C. Simo and J.W. Ju. On continuum damage-elastoplasticity at finite strains. *Computational Mechanics*, 5:375–400, 1989.

[48] M.J. van den Bosch, P.J.G. Schreurs, and M.G.D. Geers. An improved description of the exponential xu and needleman cohesive zone law for mixed-mode decohesion. *Engineering Fracture Mechanics*, 73:1220–1234, 2006.

[49] X.P. Xu and A. Needleman. Void nucleation by inclusion debonding in a crystal matrix. *Modelling and Simulation in Materials Science and Engineering*, 1:111–132, 1993.

[50] A. Needleman. A continuum model for void nucleation by inclusion debonding. *Journal of Applied Mechanics – Transactions of the ASCME*, 54:525–531, 1987.

[51] J. Oliver. Modelling strong discontinuities in solid mechanics via strain softening constitutive equations part 1: Fundamentals. part 2: Numerical simulations. *International Journal for Numerical Methods in Engineering*, 39:3575–3623, 1996.

[52] M. Ortiz and A. Pandolfi. Finite-deformation irreversible cohesive elements for three-dimensional crack-propagation analysis. *International Journal for Numerical Methods in Engineering*, 44(9):1267–1282, 1999.

[53] B.D. Coleman and M.E. Gurtin. Thermodynamics with internal state variables. *J. Chem. Phys*, 47:597–613, 1967.

[54] A.J.M. Spencer and R.S. Rivlin. Isotropic integrity basis for vectors and second-order tensors. *Arch. Rational Mech. Anal.*, 9:45–63, 1962.

[55] A.J.M. Spencer. *Theory of invariants*, chapter Continuum physics, pages 239–353. Academic Press, New York, 1971.

[56] M.E. Gurtin. *Configurational Forces as Basic Concepts of Continuum Physics*. Springer, New York, 2000.

[57] J.C. Simo, R.L. Taylor, and K.S. Pister. Variational and projection methods for the volume constraint in finite deformation elastoplasticity. *Computer Methods in Applied Mechanics and Engineering*, 51:177–208, 1985.

[58] J.C. Simo and R.L. Taylor. Quasi-incompressible finite elemente elasticity in principal stretches. Continuum basis and numerical algorithms. *Computer Methods in Applied Mechanics and Engineering*, 85:273–310, 1991.

[59] G. Alfano. On the influence of the shape of the interface law on the application of cohesive-zone models. *Composite Science Technology*, 66:723–730, 2006.

[60] J. Mosler. On variational updates for non-associative kinematic hardening of armstrong-frederick-type. *Technische Mechanik*, 30(1-3):244 251, 2010.

[61] O. Allix and A. Corigliano. Geometrical and interfacial non-linearities in the analysis of delamination in composites. *International Journal of Solids and Structures*, 36:2189–2216, 1999.

[62] Xie D. and A.M. Waas. Discrete cohesive zone model for mixed mode fracture using finite element analysis. *Engineering Fracture Mechanics*, 73:1782–1796, 2006.